L'Institut Agro Rennes-Angers

☐ **Site d'Angers** ☒ **Site de Rennes**

Année universitaire : 2023-2024 Spécialité : Ingénieur agronome Spécialisation (et option éventuelle) : Sciences halieutiques et aquacoles (Aquaculture)	**Mémoire de fin d'études** ☒ d'ingénieur de l'Institut Agro Rennes-Angers (Institut national d'enseignement supérieur pour l'agriculture, l'alimentation et l'environnement) ☐ de master de l'Institut Agro Rennes-Angers (Institut national d'enseignement supérieur pour l'agriculture, l'alimentation et l'environnement) ☐ de l'Institut Agro Montpellier (étudiant arrivé en M2) ☐ d'un autre établissement (étudiant arrivé en M2)

Etude de l'évolution du domaine myonucléaire et de la dynamique des cellules satellites au cours de la croissance musculaire de la truite arc-en-ciel

Par : Sophie DE MONTMORILLON

Soutenu à Rennes le 11/09/2024

Devant le jury composé de :

Président : Bastien SADOUL

Maître de stage : Jean-Charles GABILLARD

Enseignant référent : Bastien SADOUL

Autres membres du jury (Nom, Qualité)

Pierre-Guy MARNET, Enseignant-Chercheur

Frédéric DESSAUGE, Chercheur

Les analyses et les conclusions de ce travail d'étudiant n'engagent que la responsabilité de son auteur et non celle de l'Institut Agro Rennes-Angers

Remerciements

Je tiens à remercier en premier lieu mon maître de stage Jean-Charles Gabillard ainsi que Jérôme Bugeon qui m'ont accompagné au cours de ce stage. J'ai beaucoup appris au cours des différentes discussions que nous avons pu avoir sur la physiologie de la truite arc-en-ciel et plus particulièrement sur les processus de croissance musculaire, domaine dans lequel je possédais peu de connaissances. J'ai également acquis des compétences en bioinformatique et plus particulièrement en traitements d'images et j'ai découvert des notions relatives à l'entraînement de réseaux de neurones.
Je vous remercie également tous les deux d'avoir confirmé ma volonté de poursuivre mon parcours dans le domaine de la recherche. Enfin, merci pour vos conseils et corrections concernant la rédaction de ce rapport de stage.

Merci à Sabrina Jagot pour ses conseils et le partage de ses connaissances qui m'ont permis de débuter mon stage sur de bonnes bases.

Merci également à l'UMR STLO, en particulier Jordane Ossemond et Yann le Gouar de m'avoir accueilli et formé pour l'utilisation du confocal sur leur plateforme de microscopie. Ils m'ont permis de réaliser mes acquisitions malgré les travaux et l'indisponibilité du confocal sur le site du LPGP.

J'aimerais aussi remercier l'ensemble de l'équipe CROQ pour leur accueil et leur aide pour les expériences, en particulier Cécile qui m'a encadré au début du stage pour la partie Hybridation in situ (RNAscope) du protocole.

Enfin, merci à l'ensemble du LPGP de m'avoir accueilli et integrée dans le laboratoire.

List of abbreviations

ANR: National Research Agency

UMR: Joint Research Unit

ATP: Adenosine Tri-Phosphate

SC : Satellite cells

Pax 7 : Paired Box 7 protein

MyoD: Myoblast Determination protein 1

Myog: Myogenin

Myf-5, Myf-6: Myogenic factor 5, Myogenic factor 6

GFP: Green Fluorescent Protein

MD: Myonuclear Domain

CNN: Convolutional Neural Network

RNA: RiboNucleic Acid

CMR: Carcinogenic, Mutagenic and Reprotoxic

PAF: Paraformaldehyde

DAPI: 4',6-diamidino-2-phenylindole

PBS: Phosphate-buffered saline solution

PBST: Phosphate-buffered saline solution with Tween detergent

DMEM: Dulbecco's Modified Eagle Medium

ROI: Region of Interest

List of figures

A.Myofiber length versus fish weight. B. Myofiber volume versus fish weight.

Figure 13 - Total number of myonuclei and myonuclear domain size versus fish weight for the 32 myofibers imaged during the study. Only one fiber was imaged successfully for the 600 g weight and 1000 g weight conditions. A Wilcoxon test (non-parametrical) was performed to compare 10g and 200g conditions as the data were not normally distributed. *** p-value<0.001. A. Total number of myonuclei per fiber versus fish weight. B. Myonuclear domain (MD) size versus fish weight.

Figure 14 - Demonstration of a positive correlation between the MD size and the myofiber diameter. A Spearman correlation test was performed as data were not normally distributed. *** p-value<0.001.

Figure 15 - *Nuclei* ratio comparison between fiber's extremities (Ext parameter) and middle of the fibre (Middle parameter) for two fish weight conditions: 10 g and 200 g. A Kruskal-Wallis test was performed to make pairwise comparisons between the groups of interest. The regionalization principle is illustrated on the diagram top right (Figure 10).

Figure 16 - A diffuse staining occurred on most of the fibers imaged after using Pax7 probe in RNAscope in situ hybridization. A. 3D view of a 200g-weighed individual's myofiber acquired on the ZEISS confocal (X20). Red fluorochrome (opal 620) was used to detect Pax7+ nuclei. All the nuclei show a diffuse red staining. B. 3D view of a 10g-weighed individual's myofiber (X20, confocal). The whole fiber shows a diffuse red staining. C. View of a Z-slice of a 10g-weighed individual's myofiber. Green fluorochrome (opal 520) was used to detect Pax7+ nuclei but the same diffuse staining of the whole myofiber was observed.

Figure 17 - A. Ratio of Pax7+ myonuclei per fiber versus fish weight. Wilcox test was performed to compare the two weight conditions (n=2 for 10 g condition and n=3 for 200 g condition). B. 3D view of a 10 g trout myofiber (X20, Airyscan mode). Nuclei were stained with DAPI and Pax7 positive nuclei were detected using a red fluorochrome during RNAscope (opal 620). Zoom was made on a positive nuclei cluster. ns= not significant.

Figure 18 - A. Ratio of MyoD2+ myonuclei per fiber versus fish weight. Wilcox test was performed to compare the two weight conditions (n=5 for 10 g condition and n=3 for 200 g condition). B. 3D view of a 10 g trout myofiber (X20, Airyscan mode). Nuclei were stained with DAPI and MyoD1 positive nuclei were detected using a red fluorochrome during RNAscope (opal 620). Zoom was made on a positive nuclei cluster. ns= not significant.

Figure 19 - A. Ratio of MyoD1+ myonuclei per fiber versus fish weight. Wilcox test was performed to compare the two weight conditions (n=6 for 10 g condition and n=7 for 200 g condition). B. 3D view of a 10 g trout myofiber (X20, Airyscan mode). Nuclei were stained with DAPI and MyoD2 positive nuclei were detected using a red fluorochrome during RNAscope (opal 620). Zoom was made on a positive nuclei cluster. ns= not significant.

Figure 20 - A. Ratio of myog+ myonuclei per fiber versus fish weight. Wilcox test was performed to compare the two weight conditions (n=3 for 10 g condition and n=7 for 200 g condition). B. 3D view of a 10 g trout myofiber (X20, Airyscan mode). Nuclei were stained with DAPI and myog positive nuclei were detected using a red fluorochrome during RNAscope (opal 620). Zoom was made on a positive nuclei cluster. ns= not significant.

Figure 21 - 3D view of a 10g-weighed trout's myofiber (X20, Airyscan mode). Nuclei were stained with DAPI and MyoD1/MyoD2 duplex labelling was performed using a red fluorochrome for MyoD1+ detection and a green fluorochrome for MyoD2+ detection (7 MyoD1+/MyoD2+ nuclei were detected for a total number of 191 myonuclei on the fiber, i.e a ratio of 3.7% duplex nuclei). Duplex nuclei could be assigned to a myogenic precursor

population (i.e cluster 3 or 4 for our example), showing their stage of differentiation in the myogenic lineage.

Figure 22 – *Myogenic precursors percentage comparison between fiber's extremities (Ext parameter) and middle of the fibre (Middle parameter) for two fish weight conditions: 10 g and 200 g. A Kruskal-Wallis test was performed for each type of myogenic precursor to make pairwise comparisons between the groups of interest. None of the four non-parametric test were significative. A. Pax7+ nuclei localisation on myofibers (n=5). B. MyoD2+ nuclei localisation on myofibers (n=8). C. MyoD1+ nuclei localisation on myofibers (n=13). D. myog+ nuclei localisation on myofibers (n=10).*

List of tables

List of annex

Fiche de confidentialité et de diffusion du mémoire

Confidentialité

☑ Non ☐ Oui si oui : ☐ 1 an ☐ 5 ans ☐ 10 ans

Pendant toute la durée de confidentialité, aucune diffusion du mémoire n'est possible (1).

Date et signature du **maître de stage** (2) : 05/08/2024

(ou de l'étudiant-entrepreneur)

A la fin de la période de confidentialité, sa diffusion est soumise aux règles ci-dessous (droits d'auteur et autorisation de diffusion par l'enseignant à renseigner).

Droits d'auteur

L'auteur (3) **de Montmorillon Sophie**

autorise la diffusion de son travail (immédiatement ou à la fin de la période de confidentialité)

☑ Oui ☐ Non

Si oui, il autorise

☐ la diffusion papier du mémoire uniquement(4)

☐ la diffusion papier du mémoire et la diffusion électronique du résumé

☑ la diffusion papier et électronique du mémoire (joindre dans ce cas la fiche de conformité du mémoire numérique et le contrat de diffusion)

(Facultatif) ☐ accepte de placer son mémoire sous licence Creative commons CC-By-Nc-Nd (voir Guide du mémoire Chap 1.4 page 6)

Date et signature de l'**auteur** : 05/08/2024

Autorisation de diffusion par le responsable de spécialisation ou son représentant

L'enseignant juge le mémoire de qualité suffisante pour être diffusé (immédiatement ou à la fin de la période de confidentialité)

☒ Oui ☐ Non

Si non, seul le titre du mémoire apparaîtra dans les bases de données.

Date et signature de l'**enseignant** : 04/11/2024

Utilisation de l'Intelligence Artificielle (IA) pour la rédaction du mémoire

L'intelligence artificielle a été utilisée pour améliorer le texte ☒ Oui ☐ Non

Si oui, préciser pour quelle partie de texte et à quelles fins ?

L'IA a été utilisée à des fins de correction d'éléments de langue (vocabulaire, formulation) dans l'introduction et le matériel et méthodes du mémoire (partie 1 et 2) ainsi que dans les résultats (partie 3) pour analyser les messages d'erreurs lors du codage des macros ou du traitement de données sur R.

Toute absence de déclaration précise sera considérée comme un manquement aux règles de l'éthique scientifique.

Date et Signature de l'**auteur** :  05/08/2024

Table of contents

1. Introduction

1.1 Context

Rainbow trout (*Oncorhynchus mykiss*) is the main fish species farmed in France (80% of the aquaculture production) and one of the major salmonid species farmed worldwide (960 000 t in 2020; FAO, 2024). One of the principal breeding objectives in aquaculture production and a major source of income for fish farms is the maximization of the fish muscular growth in order to get higher mass of fish fillets that is the edible and marketable part of the fish. Understanding the underlying cellular mechanisms of rainbow trout muscular growth could help to develop a more efficient aquaculture in terms of quantity and quality.

1.2 Anatomy of the skeletal muscle tissue

1.2.1 Generalities

The majority of growth results from the accretion of muscle tissue (Mommsen, 2001). This tissue allows the performance of vital functions in the individual (locomotion, respiration, supply of nutrients to the entire organism) by converting the chemical energy from food into mechanical energy through contraction. In vertebrates, this mechanical action is enabled by the presence of specialized cells in the skeletal muscle tissue known as muscle cells. These cells are multinucleated (the skeletal muscle tissue is a syncytium), spindle-shaped, and their size increases throughout the individual's life, reaching several centimeters in length for some vertebrate species. Muscle cells are surrounded by the *endomysium* which is composed by the constituents of the basal laminae (type IV collagen, laminins, entactin, perlecan). These myofibers are grouped into bundles separated from each other by the *perimysium*, an abundant loose connective tissue containing vessels, nerves and neuromuscular spindles. The entire muscle is surrounded by the *epimysium* that joins together several bundles (McCuller et al., 2024).

1.2.2 Characteristics of myofiber types and spatial distribution

Two types of fibers are distinguished in most vertebrates, namely slow-twitch fibers (type I fibers) and fast-twitch fibers (type II fibers) that are arranged in mosaic patterns within each muscle. Their metabolism and contraction performance differ as Type II fibers have a glycolytic and anaerobic metabolism with ATP generated from glycogen, leading to high contraction rates whereas Type I fibers have an oxidative metabolism resulting in lower contraction rates. In rainbow trout and more generally in teleost, these two types have the specificity to be anatomically separated, with white muscle consisting of fast-twitch fibers and red muscle composed of slow-twitch fibers. Fast-type fibers show low levels of myoglobin and

mitochondria (anaerobic metabolism) while slow-type fibers show the opposite trend with higher rates of myoglobin and lipids (Marras et al., 2013).

The *myonuclei* in the myofibers are mostly located at the periphery of the cell just beneath the plasma membrane (Roman et Gomes, 2018) although some of them can be found deeper between the myofibrils. These *nuclei* have an oval or elongated shape and do not divide in a mature myofiber.

1.2.3 Axial muscle anatomy in teleost

In teleost, these two muscle tissues are linked to two different swimming performances. The white muscle constitutes the majority of a fish's musculature (in average 90% of the fillet mass) with fast-twitch fibers well-suited for high intensity effort such as hunting or fleeing but less resistant to fatigue. The red muscle is located under the skin along the lateral line of the fish and is often removed before commercialization as it is detrimental to marketability and generate economic losses in the aquaculture sector (Génevé et al.,2022). Slow-twitch fibers show higher resistance to fatigue and are suited for continuous movements and sustained swimming.

The proportion of the myotomal muscle that comprises slow muscle fibers differs among fish species in relation to their mode of life (Greek-Walker and Pull,1975). For example, migratory species will show a higher rate of slow-twitch fibers. Rainbow trout is an opportunistic carnivorous species that can adopt both types of swimming modes. As white muscle constitutes the majority of the fish muscle mass and has an agronomic interest, we will focus on white muscular tissue in this study.

The anatomy of the white muscle of teleost differs from mammals' muscle tissue, with muscle cells extending parallel to the longitudinal axis and throughout the length separating two myosepta (that is a connective tissue similar to the *epimysium*). This segmental structure is called the myotome.

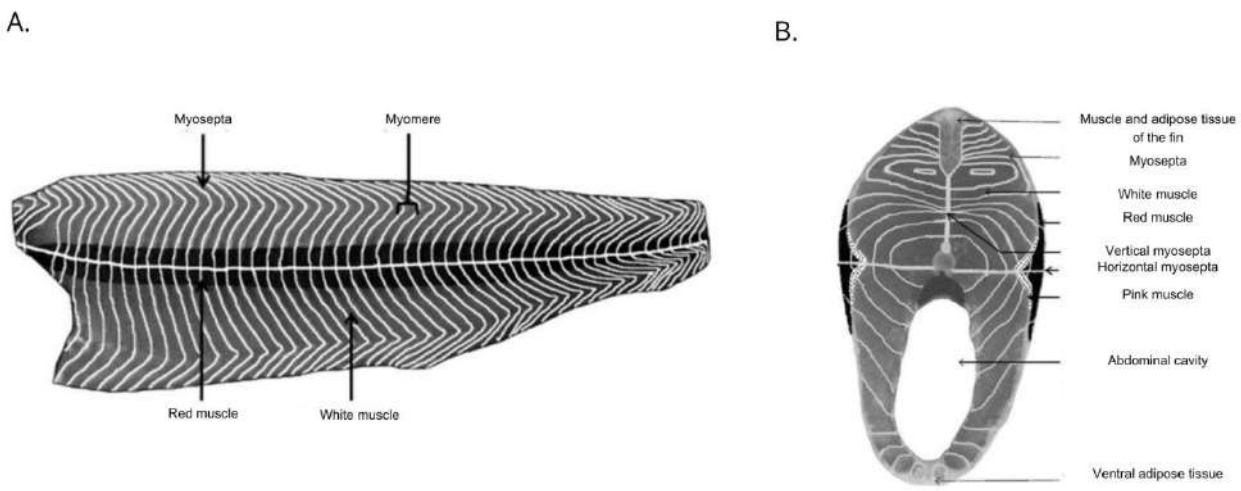

Figure 1 - *Anatomy of the axial muscle of rainbow trout:* ***A.*** *Longitudinal section of a fish fillet.* ***B.*** *Transversal section of a trout steak - macroscopic organization (adapted from Lefevre F. and Bugeon J., 2020).*

1.3 Satellite cells

1.3.1 Biological importance of adult stem cells

The establishment and regeneration of muscle tissue relies on the presence of adult muscle stem cells, capable of differentiating and self-renewing (Chazaud,2018).
Called satellite cells (18 to 50 µm in length) due to their location between the muscle fiber and the basement membrane by Mauro et al., in 1961 they have been also described in several species of fish such as trout (Steinbacher et al.,1996). These undifferentiated cells have a high nucleocytoplasmic ratio with a dense nucleus composed of abundant heterochromatin while the cytoplasm is very scant. The myogenic commitment capacity of these cells gives them a primary role in the growth and regeneration of adult skeletal muscle as they serve as a reserve for myogenic precursors for vertebrate muscle tissue. After satellite cells' activation, they proliferate and commit to the myogenic program (myoblast stage) and enter differentiation (myocyte) before fusion in myotubes. Thus, the activity and number of muscle stem cells determine the growth potential of the fish (Froehlich et al., 2013).

1.3.2 Genetic regulation of satellite cells' activity

The proliferation of these stem cells or their commitment to a differentiation pathway is regulated by gene expression. Using a model of isolated muscle fibers, it has been shown that activated satellite cells entering proliferation express both the transcription factors Pax7 and MyoD (Zammit et al., 2004). A study of a population of cells within the myotome of mouse embryos showed that Pax7 progenitor cells contribute both to muscle growth and to

maintaining a pool of stem cells. Pax7 is strongly expressed in quiescent cells involved in self-renewal and in the maintenance of satellite cell pool. Indeed, depending on the fate of satellite cells, it has been observed slight differences in Pax7 and MyoD expression. Cells that commit to terminal differentiation overexpress MyoD and repress the expression of Pax7 while cells that self-renew repress the expression of MyoD and overexpress Pax7 (Chazaud, 2018). Then, cells engaged in the differentiation pathway express in particularly the myogenin protein. Moreover, it has been shown that primary myogenic regulatory factors, such as MyoD and Myf-5 play key roles in the specification of muscle lineage, while the secondary myogenic factors, myogenin and Myf-6, are involved in differentiation.

Cellular markers Pax7, MyoD, and Myogenin (Myog) are thus extensively used to analyze the level of differentiation of myogenic precursors located on the muscle fiber (Figure 2).

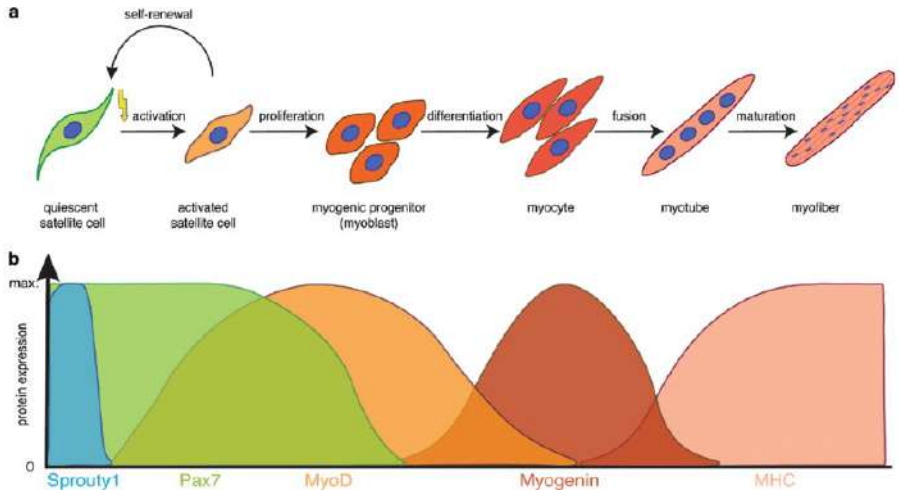

Figure 2 - *Myogenic lineage progression and expression profile of key myogenic regulators. (M. Schmidt et al., 2019)*

1.3.3 Involvement of satellite cells in muscular growth processes

Muscular growth proceeds through two main mechanisms: an increase in myofibers' size that is called hypertrophy or an increase in the number of muscle fibers called hyperplasia. After activation and commitment in the myogenic program, myocytes either fuse with another myocyte (hyperplasia) or with a pre-existing muscle fiber (hypertrophy).

Among all vertebrates, fishes appear to have specific growth patterns: first, most of the fish species, teleost included, tend to grow indeterminately (Mommsen, 2001). A key point is that there is a positive correlation between age and fish size.

Another characteristic unique to fishes is that both hyperplasia and hypertrophy contribute to post-larval muscle growth while in most other vertebrates as mammals, post-juvenile growth is through hypertrophy only (Mommsen, 2001). Teleost species as rainbow trout thus show a mosaic hyperplasia which begins at the larval stage and continues up to sexual maturation (Rescan, 2008; de Almeida et al., 2010).

The hyperplastic growth phenomenon diminishes with the age. Studies on transgenic trout expressing Green Fluorescent Protein (GFP) under the control of the Myogenin promoter— a protein expressed in differentiated muscle cells— have shown that the number of GFP-positive fibers decreases with the individual's age until they disappear after 18 months, indicating a cessation of hyperplasia (Rescan et al., 2015).

During the post-larval period (juvenile life that is the first year for rainbow trout reared under classic temperature and water conditions), the growth of trout is exponential (doubling of weight in 2 weeks between 1 and 10g) and results from very intense hyperplastic and hypertrophic activities (Stickland et al. 1983). This exponential phase is then followed by a decreasing rate of hyperplasia with a lower rate of new fibers recruited before a complete cessation above 1 kg (or an approximate length of 40 cm on Figure 3). Clearly, the formation of new fibers or the contribution to myonuclear accretion requires the action and activation of satellite cells. Interestingly, a decrease in Pax7+ cells has been observed, concomitantly with the decline in hyperplastic growth (Jagot et.al, in preparation). These results were obtained in 2D and spatio-temporal evolution of SC in muscle according to growth mode has never been studied in fish or mammals.

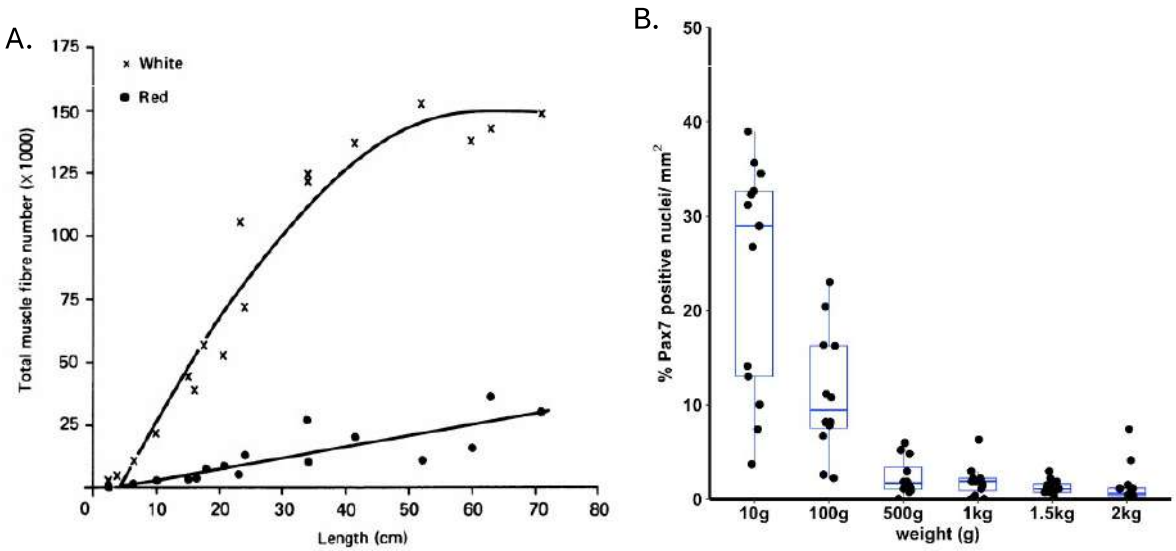

Figure 3 - A. *Total muscle fiber number in complete cross sections for white muscle and red muscle versus fish length in rainbow trout (Stickland et al.,1983).*
B. *Percentage of Pax7^{+} cells in white muscle versus trout weight (Jagot et al., in preparation).*

1.3.4 Myonuclear domain and satellite cells recruitment

Myonuclear domain (MD) can be defined as the region of cytoplasm associated with an individual *myonucleus* (Rosser et al.,2002). This region is the cytoplasmic volume that a *myonucleus* can transcriptionally govern and is calculated by dividing myofiber volume by the total number of *myonuclei* per fiber. It has been assumed that this value is constant in adult skeletal muscle with the number of *myonuclei* changing in proportion to the change in fiber size (Van der Meer et al., 2011). This implies that satellite cells are required to contribute new *myonuclei* and participate in myonuclear accretion during muscle fiber hypertrophy (Murach et al.,2017).

However, White et al. work on postnatal growth in mouse (hypertrophy) has challenged this theory. They showed that for a given developmental stage, hypertrophy occurs without myonuclear accretion, leading to an increase of the myonuclear domain size. This rises question about satellite cells implication and recruitment during maturational growth.

In rainbow trout, both hyperplasia and hypertrophy occur during juvenile muscular growth, but it has been shown that the ratio of satellite cells was decreasing with trout aging (Figure 3-B.) Myonuclear domain size evolution could be an indirect indicator of satellite cells recruitment.

1.4 Scientific relevance of the present study

Only a few studies have explored the stem cells dynamics during fish muscular growth and in particular during rainbow trout muscular growth, a specie of agronomic interest. Additionally, the hyperplasia decline has raised questions concerning the myogenic precursor's dynamics and characteristics during rainbow trout juvenile life. A recent single cell approach has allowed the identification of different populations of myogenic precursors (Figure 4) based on expression of the transcription factors mentioned above (Figure 2).

A preferential localization of positively marked Pax7 cells (characteristic of satellite cells) at the ends of muscle fibers has been observed in zebrafish (Ganassi et al., 2020) but the functional consequences remain unknown. Studying the localization and the number of these satellite cells (and each myogenic cell population) on rainbow trout white muscle fibers throughout juvenile life contributes to appreciate the cellular processes inherent to muscle growth. Moreover, analyzing myonuclear domain evolution and finding potential migration patterns of satellite cells could help understanding their recruitment.

We could imagine that it would be possible then to control and promote satellite cells' recruitment. This could help to restrict or at least delay the hyperplasic decline that occurs during the first year of rainbow trout's life leading to a maximization of muscular growth in rainbow trout farms.

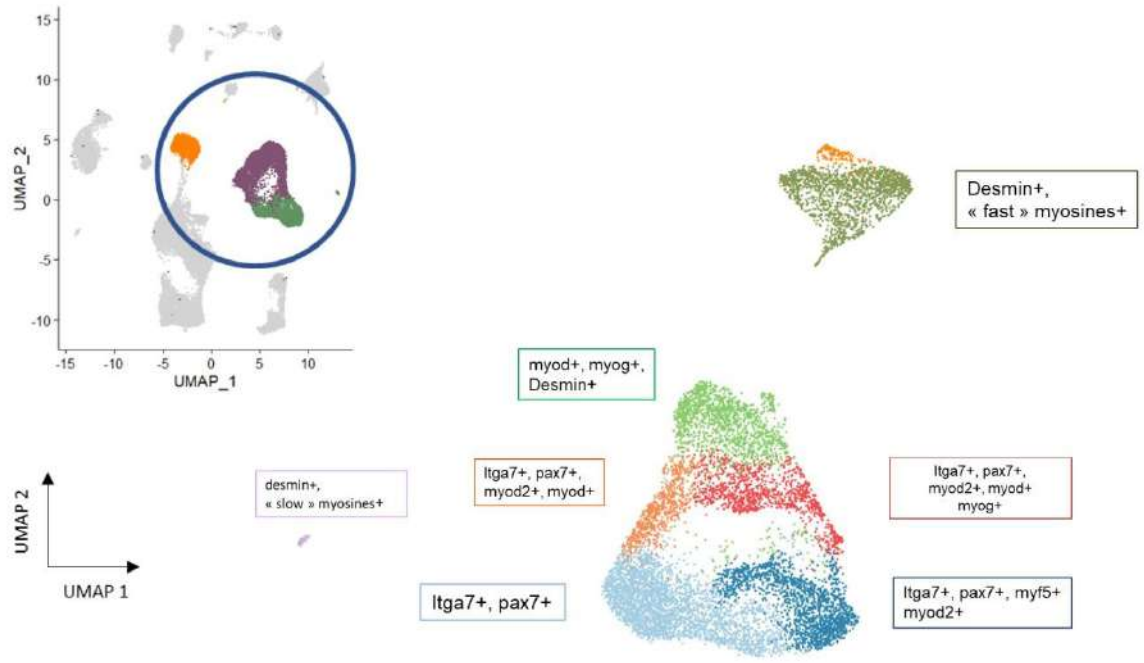

Figure 4 - *Result of white muscle single cell RNAseq analysis – eight clusters belonging to myogenic lineage have been identified at various stages between quiescent satellite cells to myocytes (Jagot et al., 2024).*

1.5 Specific objectives

The present work aims to study the evolution of the myonuclear domain during the juvenile period and to describe the satellite cells (SC) location dynamics during differentiation in trout.

The specific objectives of the present work are to develop a protocol for extraction and isolation of white myofibers in rainbow trout as well as a method for 3D-image acquisition of myofibers and *myonuclei* counting by convolutional neural network (CNN) training. Transcription factors' expression in myogenic precursors will be identified using RNA Fluorescence *in situ* hybridization.

This study is part of the FishMuSC project, financed by ANR (National Research Agency) which started in 2021 for four years. FishMuSC aims to analyze the cellular and molecular dynamics of muscle stem cells during the decline of muscle hyperplasia in trout.

2. Material and methods

2.1 Ethics statement

Rainbow trout (*Oncorhynchus mykiss*) were reared in a recirculating rearing system under natural simulated photoperiod and at 12 ± 1 °C (pH 7.8-8.4; NH4<0.1mg/L). Fish were fed daily *ad libitum* with a commercial diet (Le Gouessant) and reared at the INRAE Fish Physiology and Genomic Laboratory (LPGP) experimental facilities (DOI:10.15454/45d2-bn67, permit number D35-238-6, Rennes, France), delivered by French veterinary services. For tissue collection, fish were anesthetized with tricaine at 50 mg/L and euthanized with tricaine at 200 mg/L. All experimental procedures were carried out in strict accordance with the European Directive 2010/63/EU on the protection of animals used for scientific purposes.

2.2 General experimental design

Extraction and isolation of intact myofibers from individuals required several steps detailed below and summarized in Annex I (overall protocol). After euthanasia, the steps were conducted in the laboratory mostly under the hood following safety rules related to the handling of « Carcinogenic, Mutagenic and Reprotoxic » (CMR) substances.

2.2.1 Tissue dissection

Fishes were weighed before being dissected. Four mean weight conditions were used for the project: 10 g, 200 g, 600 g and 1000 g. Dissection was performed using a scalpel and clamps to remove skin or extract the sample. Each fish was placed on a lateral position and skin was removed from the opercula to the tail lengthwise and from the pectoral fin to two centimeters under the lateral line widthwise. Then the red muscle (the first layer under the skin) was removed. Sample of white muscle was cut lengthwise doing broad shearing movements. Only the dorsal part between two myosepta was kept from the muscle piece. The muscle fragment was then isolated in a 14 ml Falcon tube in phosphate-buffered saline (PBS) under ice.

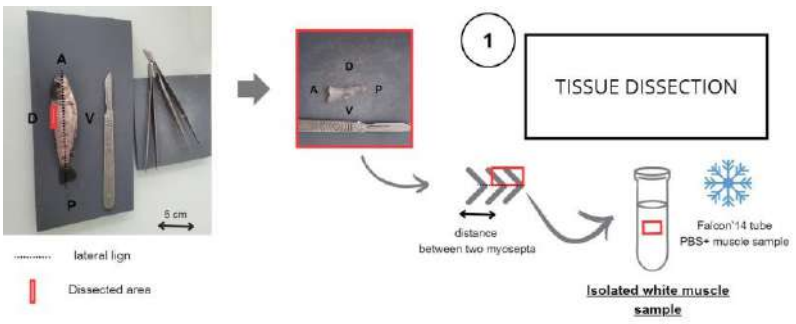

Figure 5 - *White muscle tissue dissection principle. A muscle sample was collected from the dorsal part of the fish (picture of a 10 g rainbow trout reared in the laboratory facilities).*

2.2.2 Cell fixation

Cell fixation was performed using paraformaldehyde (PAF). The fast muscle sample was fixed in 4% PAF solution on ice for two hours. This step enables immobilization of cellular components in a state as close as possible to the living state and prevents satellite cells from potential further degradations.

2.2.3 Enzymatic digestion

Muscle sample was digested in type II collagenase in order to isolate fast myofibers from the muscle tissue. A solution of 0,2% Collagenase Type II (C9891; lot :0000145780, activity = 991 U/mg) in Dulbecco's Modified Eagle Medium (DMEM) was prepared. The digestion was performed at 37°C under stirring for 30 to 45 minutes, depending on the weight of the fish: muscle sample from young individuals (mean weight being 10 g or 200 g) were kept in the digestion mix for 30 minutes while samples from older trout (mean weight being 600 g or 1 kg) were digested for 45 minutes. This difference in treatment is explained by the variation in the composition of the extracellular matrix of the muscle tissue at different ages.

After digestion, samples were immerged in a Petri dish filled with PBST (0,1%Tween, PBS) and fibers could be collected directly in the liquid using a Pasteur pipette. Fibers were kept in 1,5 mL Eppendorf tube in methanol at -20°C, with in average 30 to 40 fibers in each tube.

2.2.4 In situ Hybridization (RNAscope)

Fibers have been rehydrated (5-minutes successive baths in 50% methanol/PBS, 30% methanol/PBS and 100% PBS) before *in situ* hybridization using RNAscope Multiplex Fluorescent Reagent V2 Kit (ACDBio, ref 323100). Duplex labeling was performed using four different probes designed and synthesized by ACD Bio: Pax7, Myod1, MyoD2 and myogenin probes (references: Om-pax7b-cust (channel 1) 575461, Om-myod1C2 1039251-C2, Om-myod2-C3 1039261-C3, Om-myogenin-C3 1289381-C3). Two controls were performed using the Negative Control Probe DapB (ACD Bio,ref 310043) and the C1-collagenase probe in order to check if some *nuclei* belonged to fibroblast-like type.

After fibers' rehydratation in 1,5 mL Eppendorf tubes, fibers were incubated with Protease III for 30 minutes at 40 °C in a Bioblock oven. This step allows for the degradation of cross-links between proteins that may form during tissue fixation. The Protease treatment thus increases the permeability of the tissues to the probes.

In situ Hybridization was then performed using C. Ralliere protocol (code: MO-BIO-HIST-018,2021) (Annex II). RNAscope involves several amplification steps that enable the hybridization of Z-shaped oligonucleotides pairs of probes to the messenger RNA of interest.

Signal visualization is achieved by attaching fluorescent molecules (opals) to each target. Two Opals were used for duplex signal detection: Opal 520 (Akoya Biosciences, reference: FP1487001KT) and Opal 620 (Akoya Biosciences, reference: FP1495001KT).

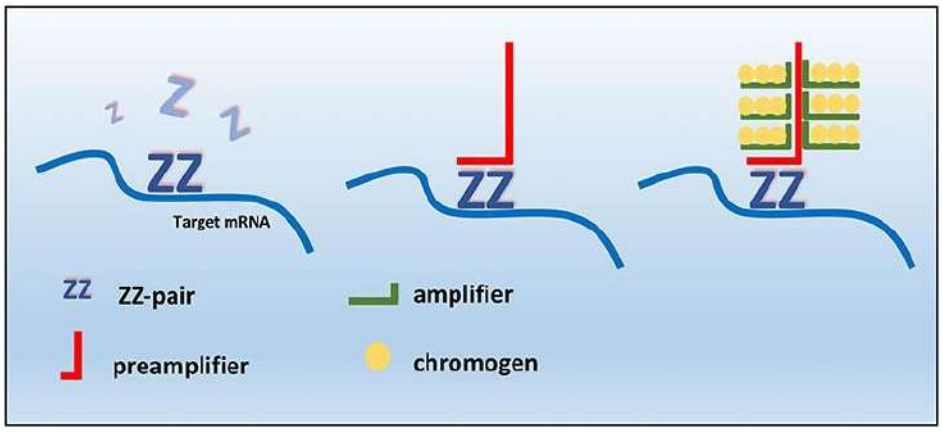

Figure 6 - *RNAscope in situ Hybridization principle (De Biase et al.,2021).*

After RNAscope, an additional labelling was performed with « 4',6-diamidino-2-phenylindole » (DAPI) to visualize all the *myonuclei* on the microscope. Fibers were put 5 minutes in a (0,01 µg/ml DAPI, PBST) solution. Fibers were washed three times before being mounted on slides for acquisition. Mounting was performed using Ecomount Biocare mounting medium (ACDBio, reference: 320409) and the hydrophobic pen Immedge (ACDBio, reference: 310018) to maintain fibers and medium in a restricted zone and to facilitate their detection for confocal acquisition. A tissue clearing step was added during mounting on slides in order to improve visualization by reducing light scattering. This step is particularly necessary for high-diameter (100-200 µm) fibers from 600g-weighed or 1000g-weighed trout. This step was performed using a 1,33 mg/L histodenz solution (Sigma-Aldrich, reference: D2158) in PBS instead of Ecomount Biocare mounting medium. By aligning the refractive indices of the tissue and the solution, Histodenz solutions improve the optical clarity of the tissue, making it easier to visualize internal structures under the microscope.

2.2.5 Acquisition of myofibers 3D-images

3D-images were acquired using the confocal microscope LSM 880 Zeiss on the STLO microscopy platform. Focusing and adjusting of the microscope was performed with the ZEN black software (ZEN 2.3 SP1) using the Tile Scan and Z-stack option to obtain a 3D-image. Airyscan mode was selected for each acquisition. Airyscan is based on a detection technology that enhances resolution and sensitivity by using an array of detectors to capture multiple images from different angles. This array allows for the collection of more detailed information about the sample's fluorescence, enhancing the signal-to-noise ratio and overall image quality. Post-processed images were visualized with ZEN Blue software.

2.3 Image analysis

All 3D-images were analyzed on FiJi (ImageJ 1.54f). Specific analyses as RNAscope-marked nuclei detection and cutting the fiber into equal part required development of a macro using ImageJ macro language.

StarDist 3D was the CNN used in this study to develop a reliable and quick *myonuclei* counting method. This CNN uses a star-convex shape model to represent the objects of interest : the segmentation process is simplified by converting the complex 3D-structure of the object into a star-convex polygon with vertices that represent the object's boundary (Weigert et al.,2020).The method has been tested with success for overlapping and touching objects and has been determined to be the best to separate and identify individual myonuclei on trout myofibers that have a relatively high nuclear density.

Quantification and further analyses were conducted on R software (version 4.3.1) using classical data analysis packages.

2.3.1 Training of the convolutional neural network (CNN) Stardist3D

Nuclei counting was performed using the convolutional neural network (CNN) Stardist3D (https://github.com/tpecot/NucleiSegmentationAndMarkerIDentification) already pretrained on generic 3D-images.

Fine-tuning was performed by training Stardist3D on a specific dataset that has been a confocal 3D-image of a 1000 g trout myofiber previously acquired in the laboratory with the SP8 -TEFOR confocal using an air objective at 25x magnification. This 3D-image (89 Z-slices) of the whole myofiber was cropped in 24 3D- images for training.

These images were annotated at the beginning of this internship using plugins on Fiji software as detailed on Figure 7. Annotated images were submitted for CNN training using Stardist3D training code on Thierry Pecot Github.

To assesses the model's performance we split the 24 3D-images data set on a training and validation datasets and measure the loss function (mae function) produced by our model on both datasets.

Loss curve was expected to decrease as the model learned to fit the training data. Validation loss reflected how well the model generalized to new unseen data by evaluating performance on a separate validation set. This parameter was critical to check that the model was not overfitting by increasing validation_loss value beyond a certain number of epochs. Finally, the validated model was the one with the lowest validation_loss value that was observed after 185 epochs (iterations). An additional validation was performed before each analysis doing an overlay between the raw 3D-image and the Stardust3D- annotated image.

Stardist3D 185 epochs-model trained on our data set was the model used for counting *myonuclei* on whole myofibers 3D-images acquired during this study.

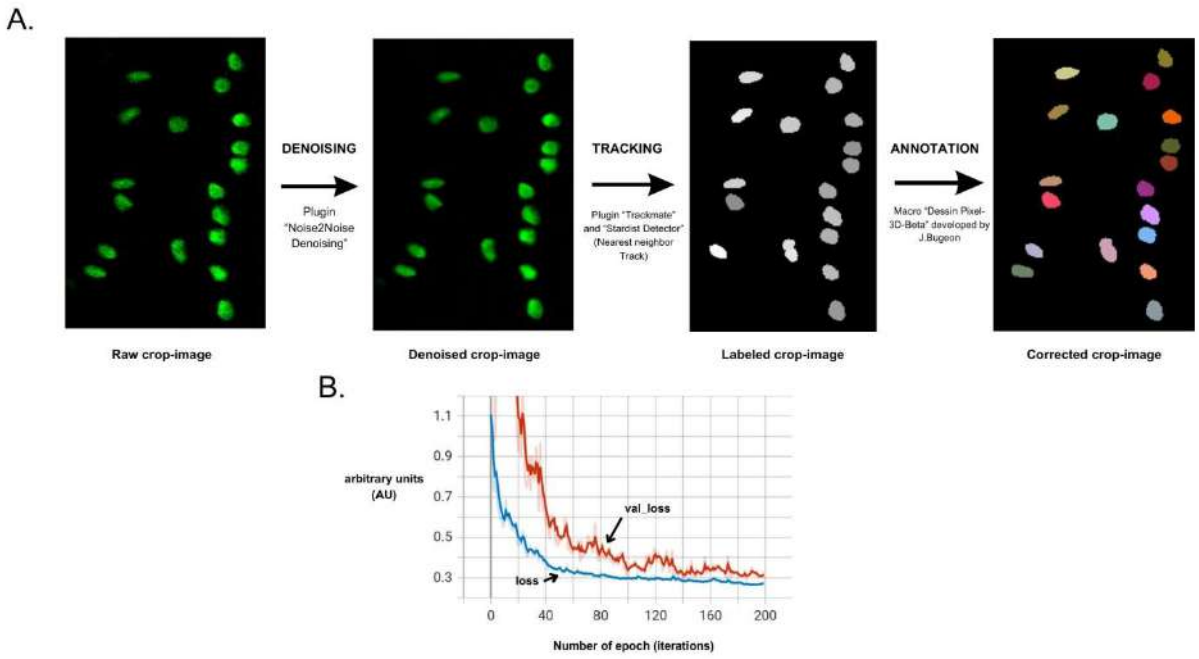

Figure 7 - *Stardist3D training (fine-tuning) principle*. ***A.*** *Overview of the main steps followed for cropped 3D-images annotation (example on one among the 24 cropped images). A green coloration was applied on nuclei for better vizualisation. Tracking step consisted of assigning a label to each nucleus detected. Annotation included detection of potential false positive or false negative labels and correction using labeling tools developed in a macro by J.Bugeon.* ***B.*** *Loss and validation_loss curves. Blue curve shows how well the model learn to fit training data. Red curve shows potential overfitting and how well the model generalizes to new unseen data.*

2.3.2 *Myonuclei* counting with Stardist3D trained model

Stardist3D was used to count *myonuclei* on whole myofiber post-processed 3D-images acquired on Zeiss confocal. As model training used an image acquired with TEFOR confocal in the laboratory, images acquired during the study were rescaled to take into account anisotropy and prevent the model from doing hallucinations.

Pre-treatment as image clearing (« Substract Background » plugin) was performed to increase the signal-to-noise ratio.

Post-processed and treated 3D-images have been used as input dataset for nuclei detection with Stardist3D. Labeled 3D-images have been stored in an output file. The plugin « MorpholibJ » on Fiji was then used to count the number of labels corresponding to the number of *myonuclei* on myofibers. Additional validation and detection of potential false

positive labels after Stardist label detection was performed by using the « Overlay » tool on Fiji between each input and output image.
This step was performed for counting the total number of *myonuclei* on each fiber (DAPI-stained *nuclei*) and also for counting the number of myogenic precursors on each fiber after RNAscope *in situ* hybridization (opal 520-stained and opal 620-stained *nuclei*).

2.3.3 Detecting positive nuclei after RNAscope

After confocal acquisition, post-processed 3D-images were treated on Fiji to detect and count positive nuclei on each myofiber: images were composed of three channels, each one assigned to one of the labeling. The first channel corresponded to the DAPI staining visualization and was used for total *myonuclei* counting on the myofiber. The two other channels corresponded to the RNAscope opal staining: red-staining (opal 620) for detection of the first probe and green-staining (opal 520) for detection of the second one. These channels were used to detect and count myogenic precursors.

Image treatment was performed on each image and each channel and consisted of three main actions. First 3D-images were cleaned using denoising plugins (« Substract Background », « Gaussian Blur »). As opal staining appeared to be much weaker than DAPI fluorescence, signal intensity had to be adjusted on each channel to optimize the signal-to-noise ratio (using « Enhance contrast » option on Fiji). Images had to be rescaled as the anistropy of STLO Zeiss confocal was not the same as the one of the TEFOR confocal used to acquire our training image for Stardist3D model.

As most of the transcriptional activity occurs in the cytoplasmic territory of a *myonucleus*, labels of the *myonuclei* were dilated by two pixels to include red fluo or green fluo staining that were in the myonuclear domain of positive *myonuclei* (that were myogenic precursors at a differentiation level depending on the probe used in the RNAscope).

A macro was coded using ImageJ macro language to filter dilated labels based on fluorescence intensity values. Another labeled 3D-image was then generated containing only positive nuclei. Counting was made using « MorpholibJ » plugin (see 2.3.2). This operation was made for red-fluorescence stained myonuclei and green-stained myonuclei (channels were split from the original post-processed image).
Red fluo-positive and green fluo-positive labeled images were then combined to detect doubly stained nuclei.

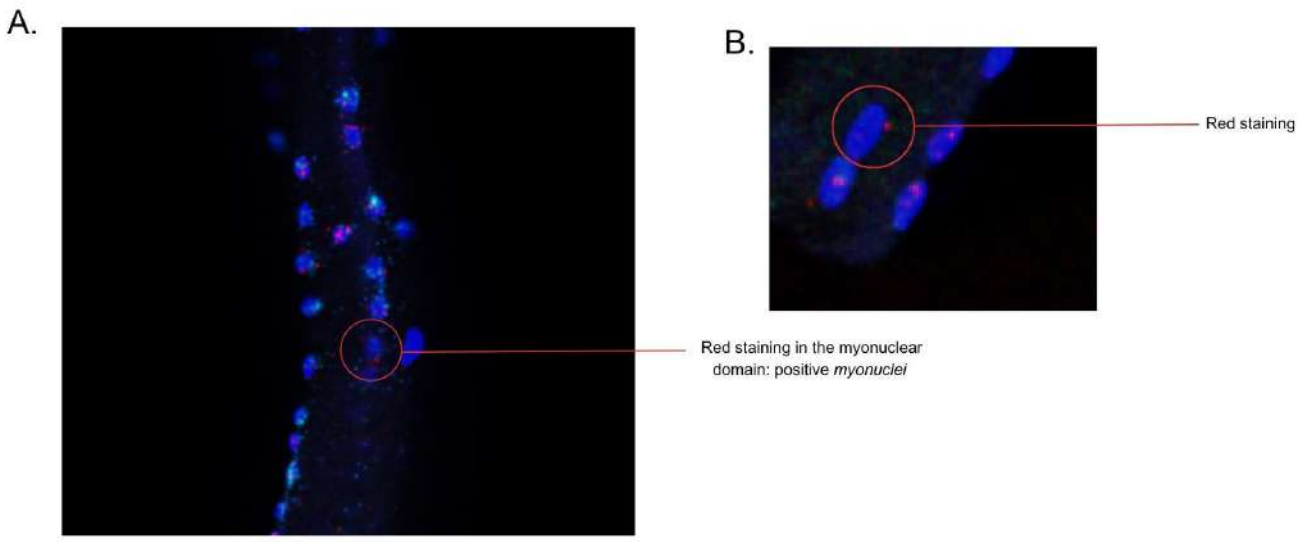

Figure 8 - *<u>Detection of positive myonuclei with fluo staining in the myonuclear domain.</u>* ***A.*** *Zoom of a 10g-weighed trout's myofiber section before label dilatation. Red stained was included in the label after the two-pixel nuclei dilatation process.* ***B.*** *Zoom on a smaller section of the myofiber. The circled nuclei were considered as a myogenic precursor as red staining was seen in the myonuclear domain.*

2.3.4 Measure of the myofiber volume

In order to analyze the myonuclear domain evolution, a protocol was developed to calculate a myofiber volume on a 3D-image on Fiji (most plugins were adapted to 2D-images). This protocol was based on detecting the whole myofiber as a label in order to use « MorpholibJ » plugin and calculate the label volume. Myonuclear domain (MD) was then deduced from the total number of *myonuclei* using the formula below:

$$MD\ (x\ 10^{3}\ \mu m^{3}) = \frac{\text{Myofiber Volume } (x\ 10^{3}\ \mu m^{3})}{\text{Number of myonuclei}}$$

Parameters that were considered for the analysis to study muscular growth and nuclei accretion were myofiber volume, total number of myonuclei, myonuclei density and myofiber length.

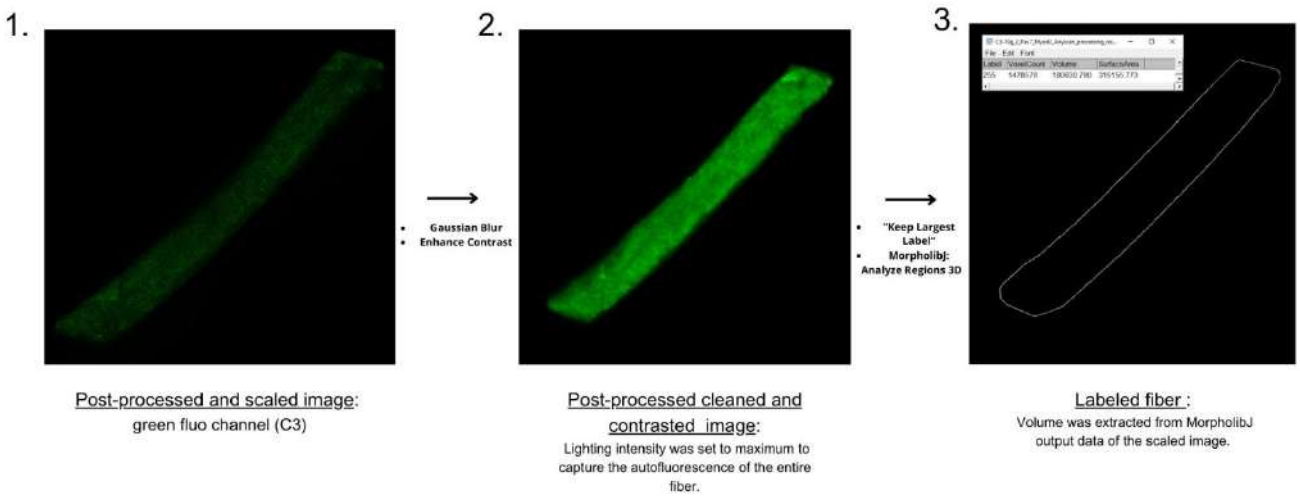

Figure 9 - *Myofiber Volume calculation process summarized in three steps. Example is a Z-slice from a C3-channel 3D-image of a 10g-weighed trout's myofiber after a duplex RNAscope (Pax7 probe/Myod2 probe).* ***1.*** *Image was scaled, and channels were split to keep only the third channel.* ***2.*** *The image was cleaned and contrasted (maximum intensity).* ***3.*** *Image was labeled using thresholding parameter and the largest label corresponding to the whole fiber was kept. Computation of all the Z-slices with MorpholibJ gave the label volume.*

2.3.5 Virtual cutting of the myofiber in equal parts

A macro was developed using ImageJ macro language on Fiji in order to analyze the myogenic precursors localization on each myofiber. Fibers were virtually cut in four equal parts: zone 1 and 4 corresponded to myofiber's extremity (extern part) and zone 2 and 3 to the middle of the myofiber (intern part). As the fibers were assumed not to have a specific direction, zone 1 and 4 were combined in an extern zone and similarly zone 2 and 3 were combined in an intern part to expand the sample size and improve the statistical validity of our results.

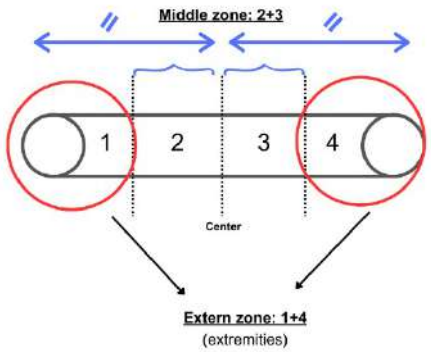

Figure 10 - *Principle of the virtual cut of a myofiber. The fiber was modeled as a cylinder.*

Most of the fibers were curved and inclination angles had to be taken into account when coding the macro for sectioning. A region of interest (ROI) was manually drawn on Fiji to select the

whole fiber. The coordinates of the three cutting lines were determined by calculating orthogonal projections in the macro.

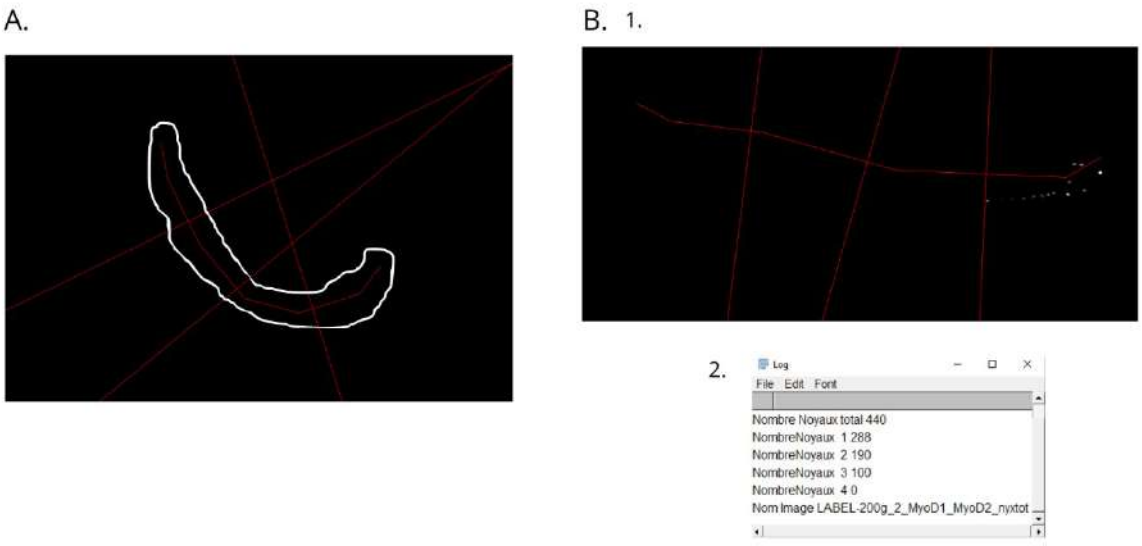

Figure 11 - A. *Illustration of the sectioning ROI plotted with the macro (input is a 10 g trout myofiber labeled 3D-image). Virtual contours of the fiber have been added to explain the fiber length's ROI outline.* ***B.1.*** *The macro's principle is based on counting myonuclei (with MorpholibJ) in each fiber zone defined by the sectioning ROI.* ***B.2.*** *The macro-output table gives the total number of nuclei in each zone and in the entire fiber.*

The number of *myonuclei* was calculated in each zone using MorpholibJ. This process was applied for total number of *myonuclei* from one hand and for myogenic precursors' *nuclei* on the other hand.

2.4 Statistics

All data analyses were realized with RStudio, version 4.3.1.

Classical data analysis packages were used and non-parametric tests were performed to compare results between our groups of interest due to the very small sample size and the presence of extreme values in our data. Wilcoxon test for pairwise comparisons and Kruskal-Wallis test for multiple comparisons were chosen for their robustness to the assumptions about data distribution.

3. Results

3.1 Development and optimization of a protocol for extraction and isolation of entire fast-twitch myofibers and 3D-images acquisition

A protocol summarized in appendix I was developed for this study. This protocol is based on a preliminary trial from which each step was optimized, but Enzymatic Digestion (step 3) and Image Acquisition (step 5) required more optimization.

Enzymatic digestion for isolation of myofibers from the muscle sample was performed using type II collagenase. Different incubation parameters and solvents were tested, and the optimal incubation conditions were defined following the digestion efficiency: the number of intact myofibers isolated from the tissue per sample was looked at for each digestion condition. The optimal conditions were found to be an incubation in a (0,2% type II collagenase, DMEM) solution at 37°C under stirring for 30 minutes (10 g and 200 g trout) to 45 minutes (600 g and 1 kg trout). A simple RNAscope *in situ* hybridization was performed using Pax7 probe to detect satellite cells (SC) on myofibers and check that enzymatic digestion did not provoke SC detachment. It would have been interesting to test the washing medium to verify that it did not contain any satellite cells.

Acquisition of 3D-images required the use of a fluorescence microscope. The *myonuclei* detection deep learning model Stardist3D had been trained on a fiber previously imaged on the laboratory (confocal microscope SP8). Unfortunately, this microscope was unavailable throughout the study and other microscopy methods were tested to find the most adapted one to the requirement of our study: i) a 3D acquisition on high-diameter objects ii) a good *myonuclei* resolution in order to be detected by Stardist3D and iiii) a moderate acquisition time to increase the sample size.

Table 1 - *Summary of the fluorescence microscopy techniques tested. The confocal used for this study has been the Confocal LSM 880 Zeiss airyscan at UMR STLO*

Type of microscopy	Pros	Cons
Lightsheet	• Acquisition speed • Possibility to image several fibers at the same time.	• Complex setup to develop (design of specific molds for fibers) • High-volume images (> 50 Ga) • The image resolution was low and led to hallucinations of Stardist3D model.
Confocal 3D scanner	• Acquisition speed: 12 slides/rack	• Microscope focusing was impossible (high-diameter fibers, working distance of the objectives)
Spinning Disk	• Microscope availability • Acquisition speed (higher than a confocal)	• Working distance (focusing problems) • *stitching* errors (LEICA software issues)
SP5 confocal microscope	• Microscope availability	• Working distance of objectives • Lower resolution than with a SP8 confocal (LPGP)
Confocal LSM 880 Zeiss airyscan (UMR STLO)	• Microscope availability • *Myonuclei* detection by Stardist 3D was validated • Acquisition speed + higher image resolution with Airyscan mode	• Need to optimize the protocol for mounting on slides before acquisition.

3.2 The myonuclear domain size is increasing during juvenile muscular growth

3.2.1 Evolution of fiber characteristics during juvenile muscular growth

For all the parameters studied, huge variabilities were observed between fibers from the same fish mean body weight, leading to large standard deviation values. These numeric values showing variability was supported by observations at the microscope which revealed very different fibers' size.

The measurement of myofiber length and volume showed differences according to fish weight, the 200 g trout having the more heterogenous fiber length and volume. Myofiber length and volume were significatively different between 10 g trout and 200 g trout with p-value < 0.001 for both parameters. Mean myofiber length values increased with trout weight, from 930 ± 118 µm at 10 g to 1773 ± 440 µm at 200 g. Similarly, mean volume increased from 354 ± 292 x 10^3 μm^3 to 2710 ± 2433 x 10^3 μm^3.

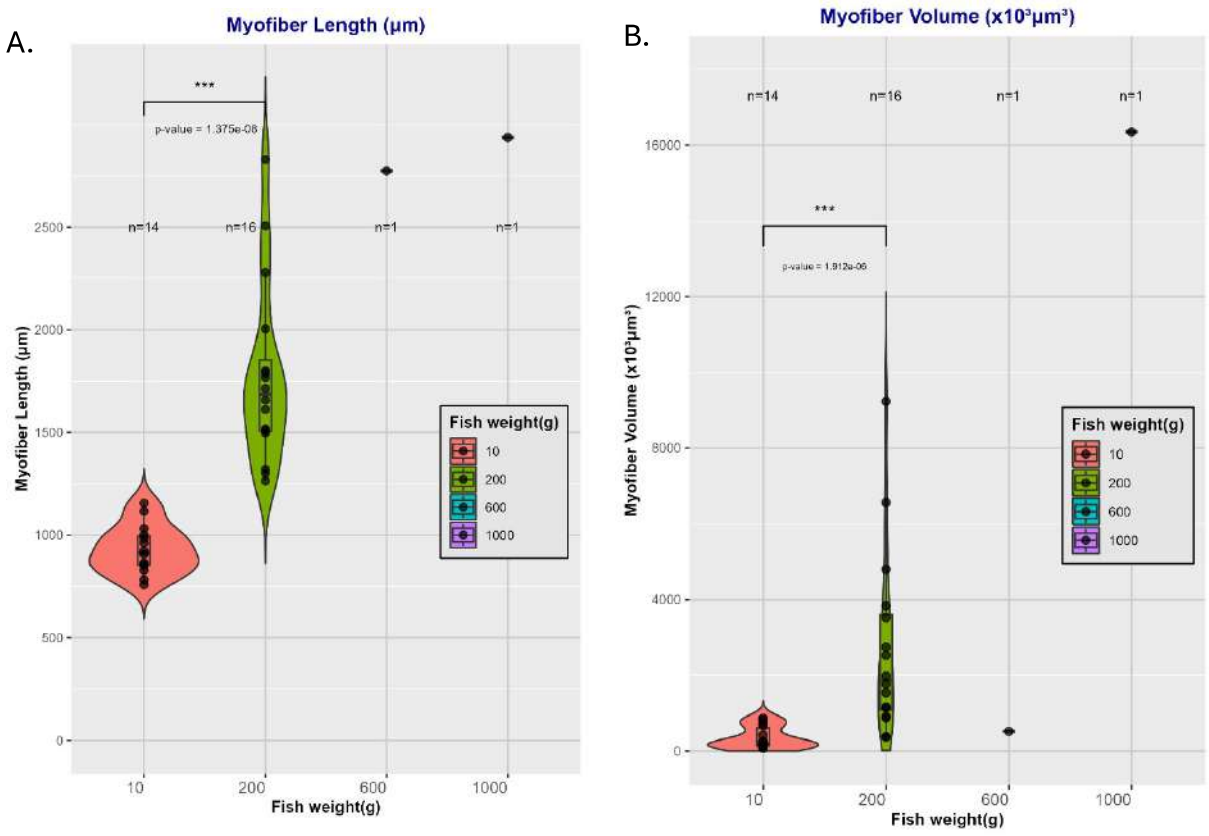

Figure 12 - *<u>Myofiber length and volume versus fish weight for the 32 myofibers imaged during the study</u>. Only one fiber was imaged successfully for the 600g-weighed and 1000g-weighed conditions. A Wilcoxon test (non-parametrical) was performed to compare 10g and 200g conditions as the data were not normally distributed. *** p-value<0.001.*

A. *Myofiber length versus fish weight.* ***B.*** *Myofiber volume versus fish weight.*

The total number of *myonuclei* per fiber was significantly higher (p-value <0.001) for fibers from 200 g trout than for fibers from 10 g trout with mean values ranging from 204 ± 67 to 588 ± 324.

The myonuclear domain (MD) size was calculated directly from the total number of nuclei and from the myofiber volume, a significative increase was observed between 10 g and 200 g trout for this parameter, from 2.21 ± 2.47x 10 ^{3} µm^{3} to 4.98 ± 4.22x 10 ^{3} µm^{3}.

The unique fiber acquired for the 600 g condition had a volume (517 x 10 ^{3} µm^{3}) similar to 10 g trout myofibers but with a relatively high myofiber length and total number of myonuclei (2773 µm, 958 nuclei) and consequently a low MD size (0.54 x 10 ^{3} µm^{3}).

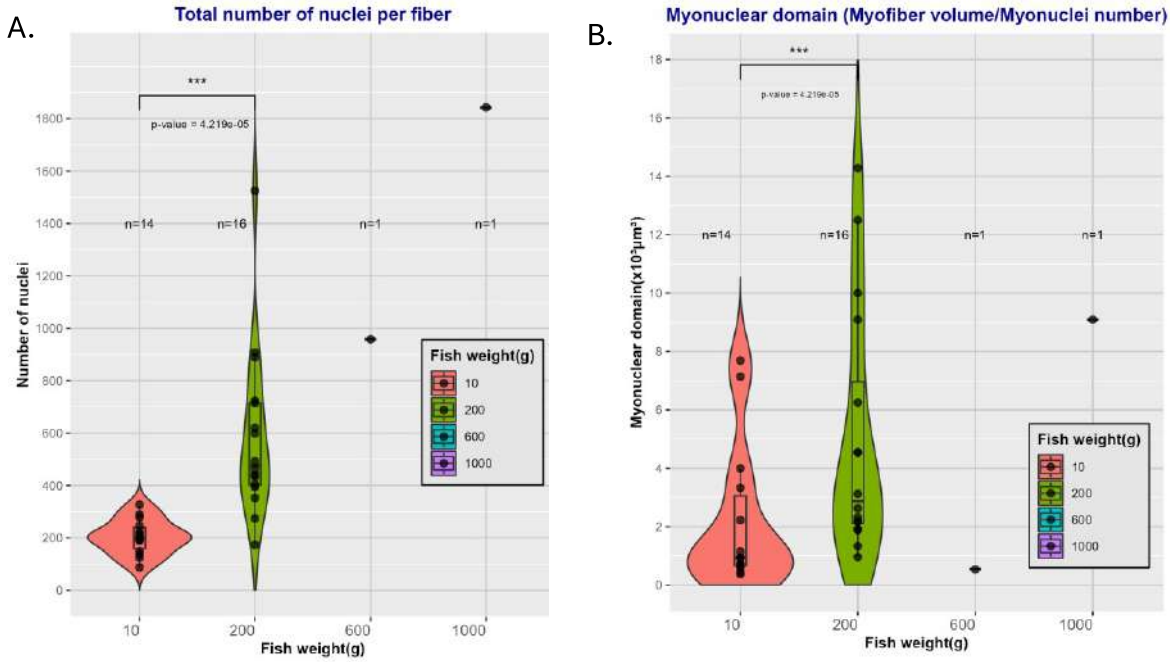

Figure 13 - *Total number of myonuclei and myonuclear domain size versus fish weight for the 32 myofibers imaged during the study. Only one fiber was imaged successfully for the 600 g and 1000 g weight conditions. A Wilcoxon test (non-parametrical) was performed to compare 10 g and 200 g conditions as the data were not normally distributed. *** p-value<0.001.*
A. *Total number of myonuclei per fiber versus fish weight.* ***B.*** *Myonuclear domain (MD) size versus fish weight.*

Myofiber diameter was calculated with the myofiber volume and myofiber length assuming that the fibers were cylindrical. A very strong positive correlation was found between MD size and myofiber diameter (p-value <0.001, rho = 0.93).

The 600 g trout myofiber showed the same values 10 g trout myofibers on the graph as some 200 g trout myofibers, although a huge variability was observed for this condition.

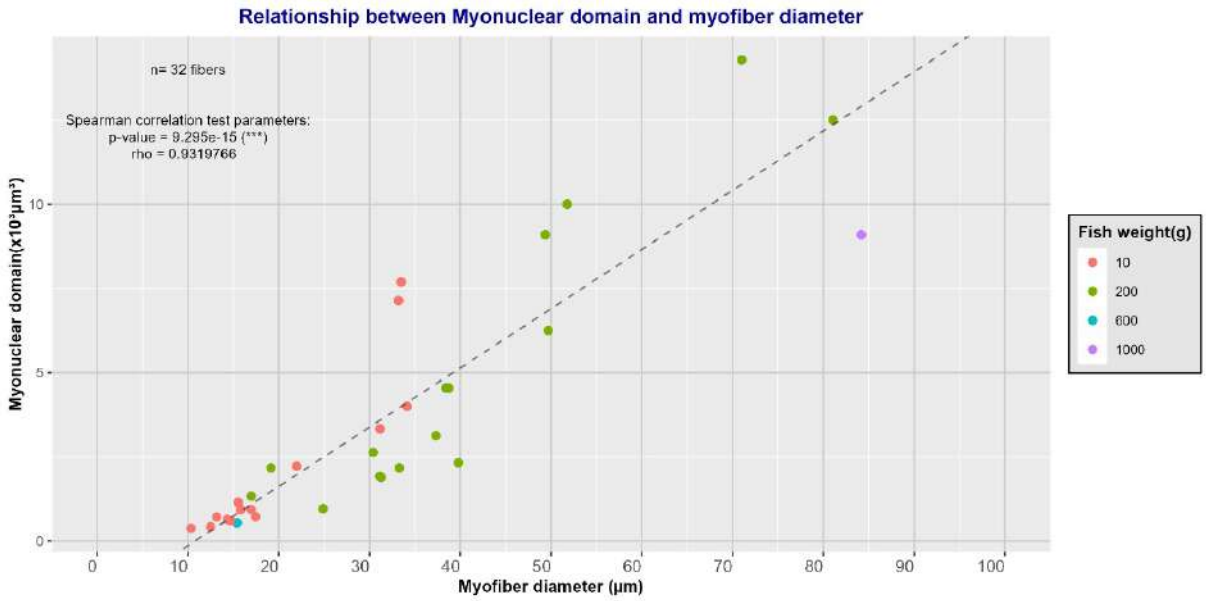

Figure 14 - *Demonstration of a positive correlation between the MD size and the myofiber diameter. A Spearman correlation test was performed as data were not normally distributed. *** p-value<0.001.*

3.2.2 The nuclei were evenly distributed along the myofibers

Analysis of the spatial distribution of *myonuclei* along the myofiber indicated that in 10 g fish myofibers, 52.1% and 47.9% of nuclei were located in the exterior and middle zone, respectively. In 200 g trout, the same nuclei distribution was observed.

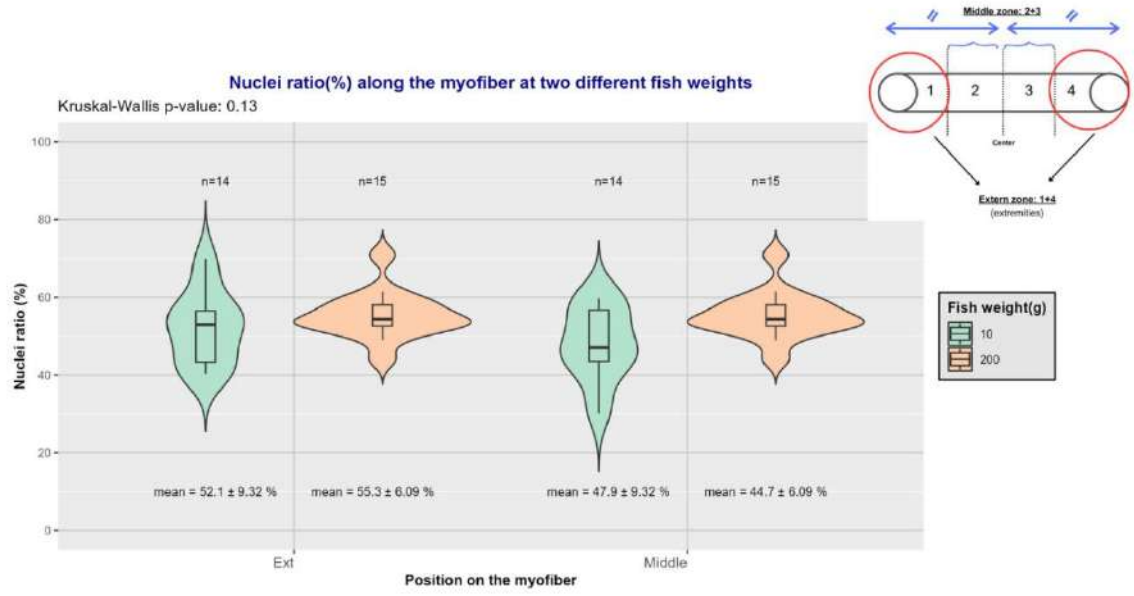

Figure 15 - *Nuclei percentage comparison between fiber's extremities (Ext parameter) and middle of the fiber (Middle parameter) for two fish weight conditions: 10 g and 200 g. A Kruskal-Wallis test was performed to make pairwise comparisons between the groups of interest. The regionalization principle is illustrated on the diagram top right (Figure 10).*

3.3 Evolution of the myogenic precursors' percentage during juvenile muscular growth

3.3.1 Development of a multiplex in situ hybridization for marker of satellite cells differentiation stages.

Several probes used for the detection of nuclei involved in myogenic programs at different stages have been used. Simple *in situ* hybridization was performed to validate the four probes used in this study.

Duplex labeling was then performed and all combinations possible were tested in order to assign myogenic precursors to clusters found on RNAseq single cell regarding their transcriptional activity (Figure 4).

Negative control was performed using a dapB probe (targets bacterial RNA sequence), and no labeled *nuclei* were observed. It confirmed that the fluorescence signal was not due to non-specific hybridization.

Another control was performed with a C1-collagen probe used to detect nuclei expressing the type I collagen, characteristics of connective tissue cells such as fibroblasts.

Only a few (less than 2%) of labeled nuclei were observed when the C1-collagen probe was used so it has been checked nuclei belonged to myofibers and not to the fibroblasts present in the connective tissue surrounding the myofibers.

Whereas the signal was always specific for MyoD1, MyoD2 and myogenin with locate puncta or intense fluorescence dots, a diffuse staining was observed on most of the fibers labeled with Pax7 probe, whatever the fluorophore used, opal 520 or opal 620 (Figure 12). These myofibers could not be analyzed as it was impossible to have a clear localization of the Pax7+ nuclei. This led to a reduction of the sample size for Pax7 condition (myogenic precursors proliferating) as 12 of the 17 fibers (71%) imaged after a Pax7 labeling were excluded from the analysis.

A. B.

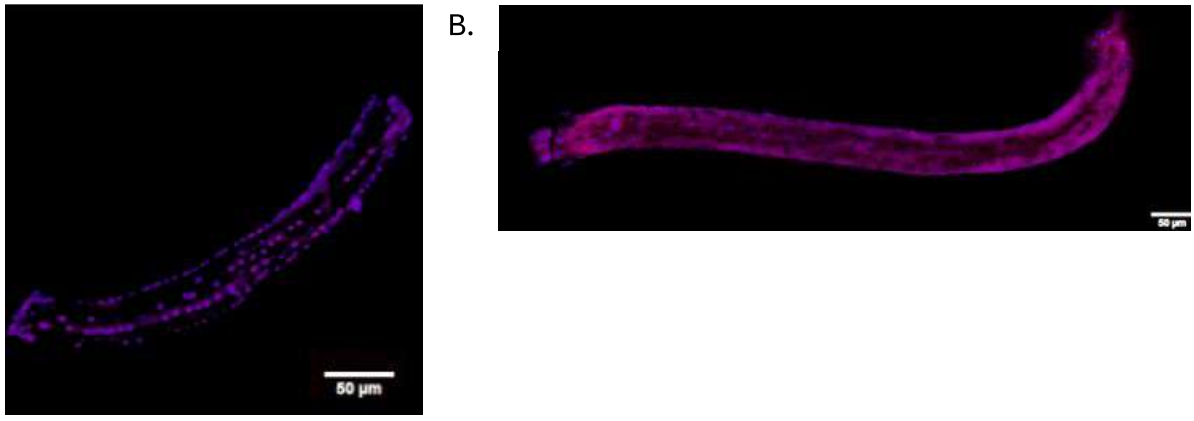

Figure 16 - *A diffuse staining occurred on most of the fibers imaged after using Pax7 probe in RNAscope in situ hybridization*. ***A.*** *3D view of a 200 g trout myofiber acquired on the ZEISS confocal (X20). Red fluorochrome (opal 620) was used to detect Pax7+ nuclei. All the nuclei show a diffuse red staining.* ***B.*** *3D view of a 10 g trout myofiber (X20, confocal). The whole fiber shows a diffuse red staining.*

3.3.2 Percentage of Pax7+ *myonuclei* per fiber

In situ hybridization on fibers were performed with a Pax7 probe to detect myogenic precursors in early stage of the myogenic program. No significant differences for the Pax7+ nuclei proportion were observed between the two 10 g trout myofibers imaged and the three from the 200 g condition (p-value =0.8). Mean values for the ratio of Pax7+ *nuclei* were respectively 14.3 ± 2.69 % and 11 ± 15 % but a huge variability was observed for 200 g trout myofibers.

A.

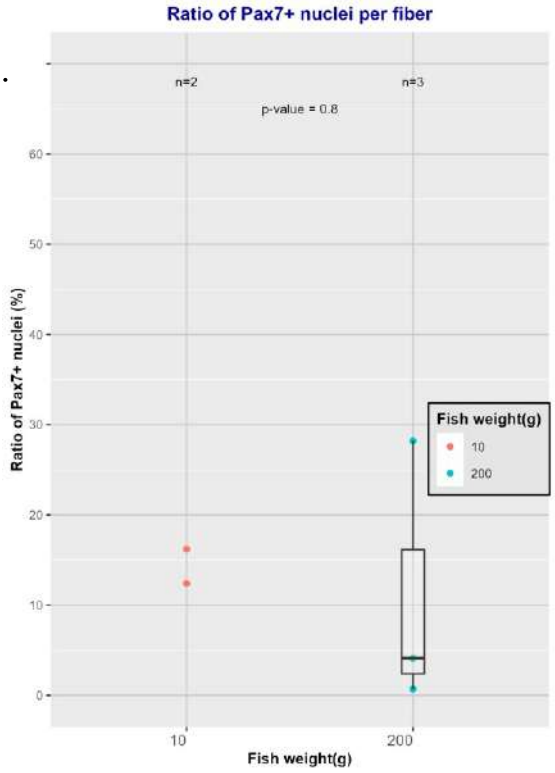

B.

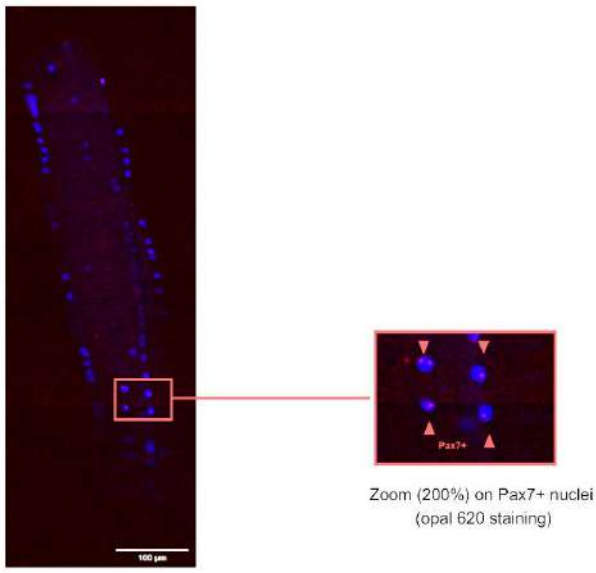

Figure 17 - A. *Ratio of Pax7+ myonuclei per fiber versus fish weight. Wilcox test was performed to compare the two weight conditions (n=2 for 10 g condition and n=3 for 200 g condition).* ***B.*** *3D view of a 10 g trout myofiber (X20, Airyscan mode). Nuclei were stained with DAPI and Pax7 positive nuclei were detected using a red fluorochrome during RNAscope (opal 620). Zoom was made on a positive nuclei cluster. ns= not significant.*

3.3.3 Percentage of MyoD2+ *myonuclei* per fiber

A MyoD2 probe was used to detect precocious myoblast (activated satellite cells). No significative differences were observed between the two weight conditions (p-value =0.5714). A huge variability was observed for both conditions with mean values being respectively 13.4 ± 8.32 % and 12.3 ± 16.40 %.

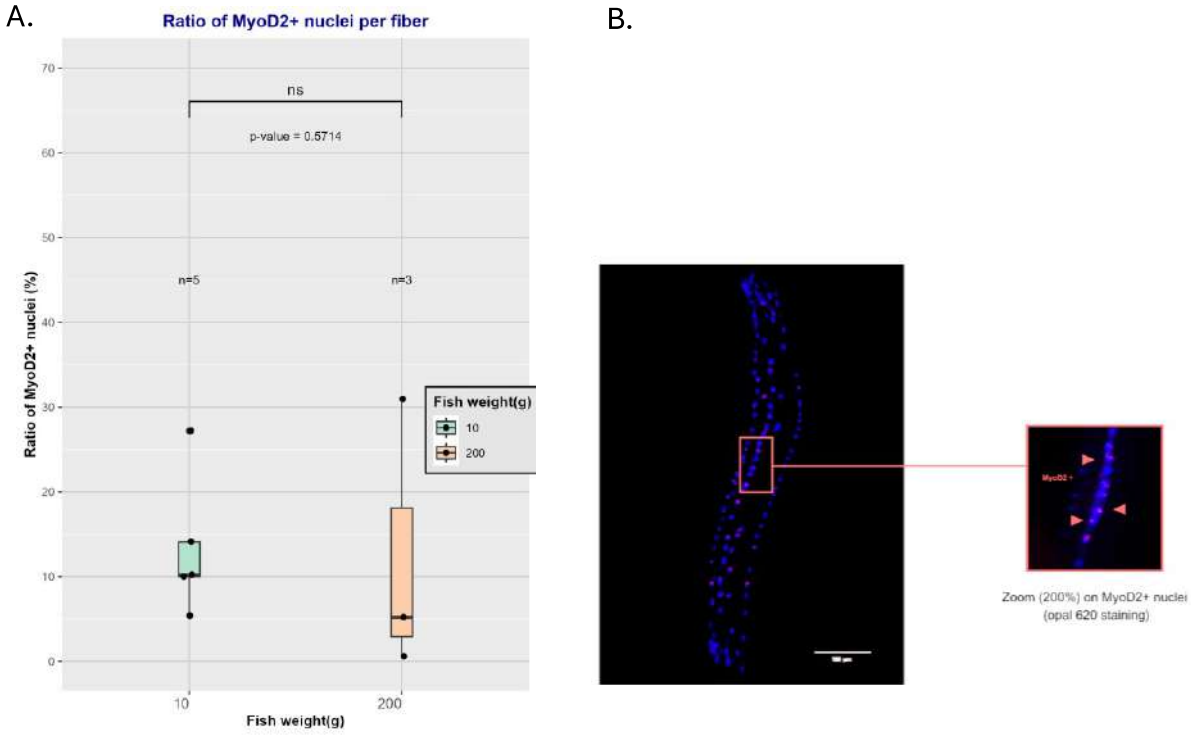

Figure 18 - A. *Ratio of MyoD2+ myonuclei per fiber versus fish weight. Wilcox test was performed to compare the two weight conditions (n=5 for 10 g condition and n=3 for 200 g condition).* ***B.*** *3D view of a 10 g trout myofiber (X20, Airyscan mode). Nuclei were stained with DAPI and MyoD1 positive nuclei were detected using a red fluorochrome during RNAscope (opal 620). Zoom was made on a positive nuclei cluster. ns= not significant.*

3.3.4 Percentage of MyoD1+ *myonuclei* per fiber

RNAscope *in situ* hybridization with a MyoD1 probe was performed to detect committed myoblasts (Figure 4). The fibers analyzed showed a relatively high proportion of MyoD1+ *myonuclei* on myofibers but no difference was observed between fibers of 10 g and 200 g trout (22.9 ± 10.2 % and 18.7 ± 11.8 %, respectively).

A.

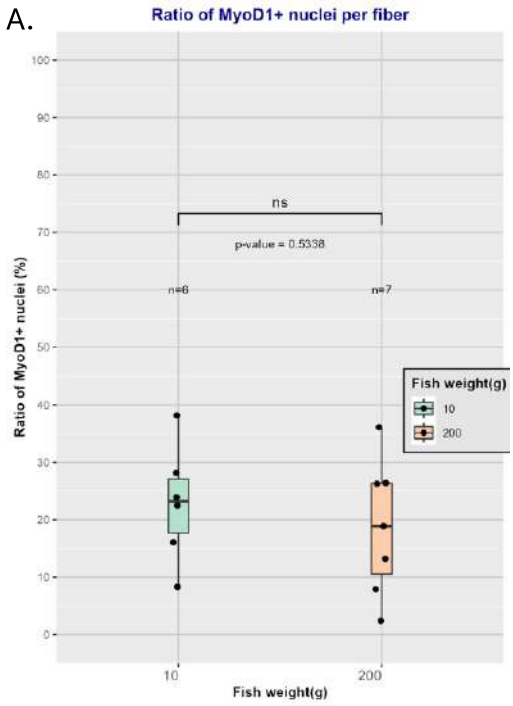

B.

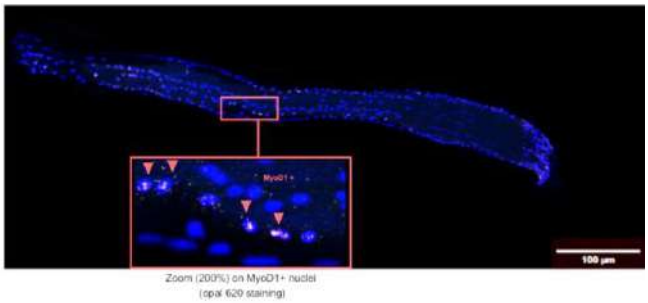

Figure 19 - A. *Ratio of MyoD1+ myonuclei per fiber versus fish weight. Wilcox test was performed to compare the two weight conditions (n=6 for 10 g condition and n=7 for 200 g condition).* ***B.*** *3D view of a 200 g trout myofiber (X20, Airyscan mode). Nuclei were stained with DAPI and MyoD2 positive nuclei were detected using a red fluorochrome during RNAscope (opal 620). Zoom was made on a positive nuclei cluster. ns= not significant.*

3.3.5 Percentage of myog+ *myonuclei* per fiber

RNAscope *in situ* hybridization with a Myogenin probe was performed to detect myogenic percursors in a more differentiated level than MyoD2+ positive cells (Figure 4). No significative differences were found between fibers of 10 g and 200 g trout (14.0 ± 2.85 % and 9.1 ± 5.64%). Results of the non-parametrical test did not allow us to conclude on a significative difference between the two conditions (p-value =0.5338).

A. B.

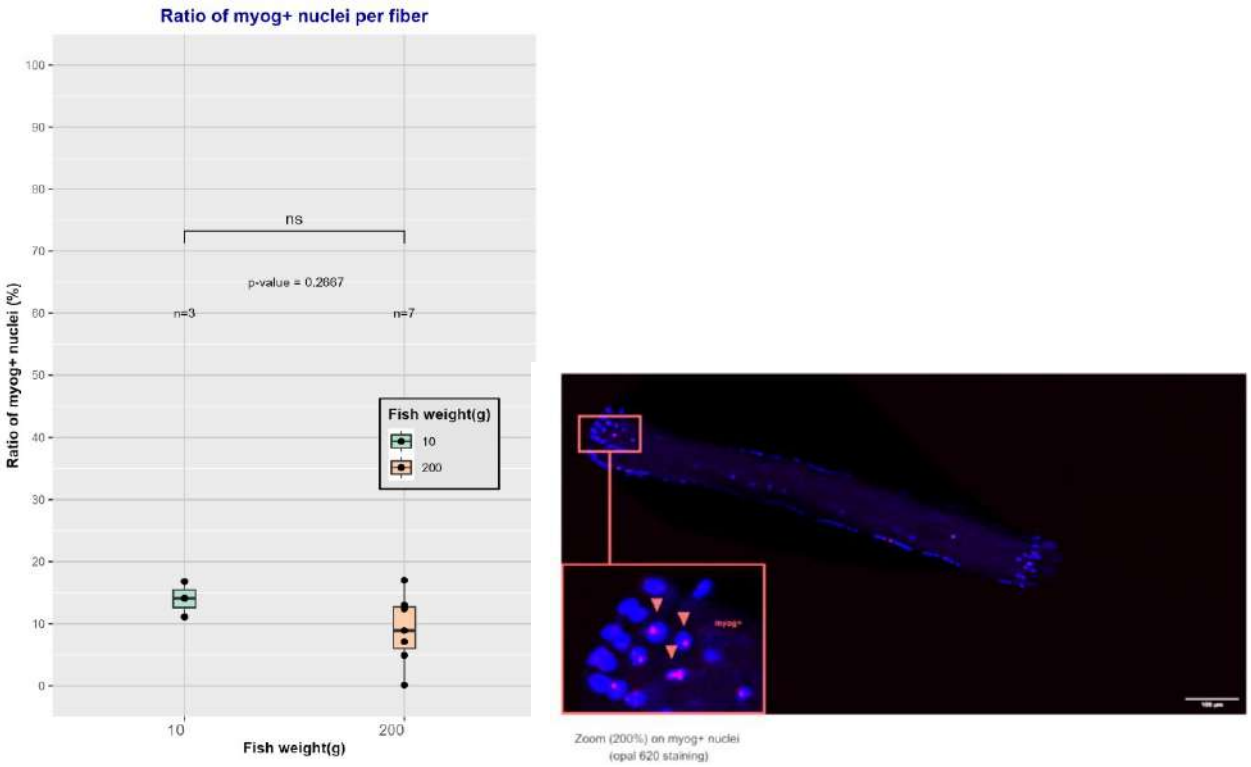

Figure 20 - A. *Ratio of myog+ myonuclei per fiber versus fish weight. Wilcox test was performed to compare the two weight conditions (n=3 for 10 g condition and n=7 for 200 g condition).* ***B.*** *3D view of a 10 g trout myofiber (X20, Airyscan mode). Nuclei were stained with DAPI and myog positive nuclei were detected using a red fluorochrome during RNAscope (opal 620). Zoom was made on a positive nuclei cluster. ns= not significant.*

3.3.6 Duplex labelling was performed to validate all possible combinations of probes

RNAscope was performed with duplex hybridization using two different probes labeled with distinct fluorescent markers (red fluorescence, opal 620 and green fluorescence, opal 520). This molecular technique aimed to detect simultaneously two different RNA targets among the four of interest (Pax7, MyoD2, MyoD1 and myog) and analyze co-expression of genes in *myonuclei*. Then, double labeled *nuclei* could be assigned to one of the clusters of myogenic precursors defined by single cell RNAseq analysis. MyoD2 and myog probes could be visualized only with opal 620 under the microscope so the duplex hybridization MyoD2/myog could not be tested. The five other combinations with the four probes of interest for this work were tested and validated on fibers (Pax7/MyoD1, Pax7/MyoD2, Pax7/myog, MyoD1/MyoD2, MyoD1/myog).

As only 15 fibers were duplex hybridization-validated for both weight groups combined and the five possible duplex combinations, no statistical analysis were made on duplex nuclei ratio per fiber or localization as the number of double positive nuclei per fiber was extremely low (in

average 15 ± 21 duplex nuclei per fiber including an outlier fiber showing 74 duplex-positive nuclei).

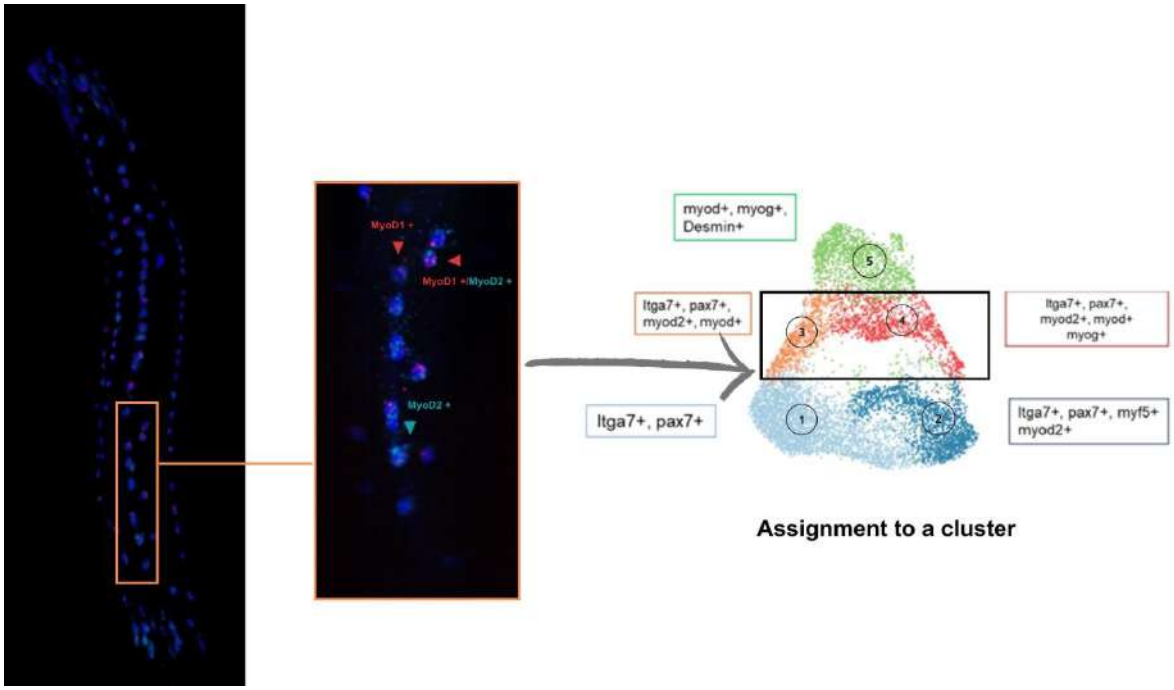

Figure 21 - *3D view of a 10 g trout myofiber (X20, Airyscan mode). Nuclei were stained with DAPI and MyoD1/MyoD2 duplex labelling was performed using a red fluorochrome for MyoD1+ detection and a green fluorochrome for MyoD2+ detection (7 MyoD1+/MyoD2+ nuclei were detected for a total number of 191 myonuclei on the fiber, i.e a ratio of 3.7% duplex nuclei). Duplex nuclei could be assigned to a myogenic precusor population (i.e cluster 3 or 4 for our example), showing their stage of differentiation in the myogenic lineage.*

3.4 Myogenic precursors of different stages were evenly distributed along the myofibers

The same localization analysis than the one made on the total number of *myonuclei* (see 3.2) per fiber was performed for each type of myogenic precursor detected with the four RNAscope probes. No significative differences were found between the two trout's age conditions and the fiber's area (middle or extremities) for each of the four probes used in this study (results of Kruskal-Wallis test showed a p-value > 0.05).

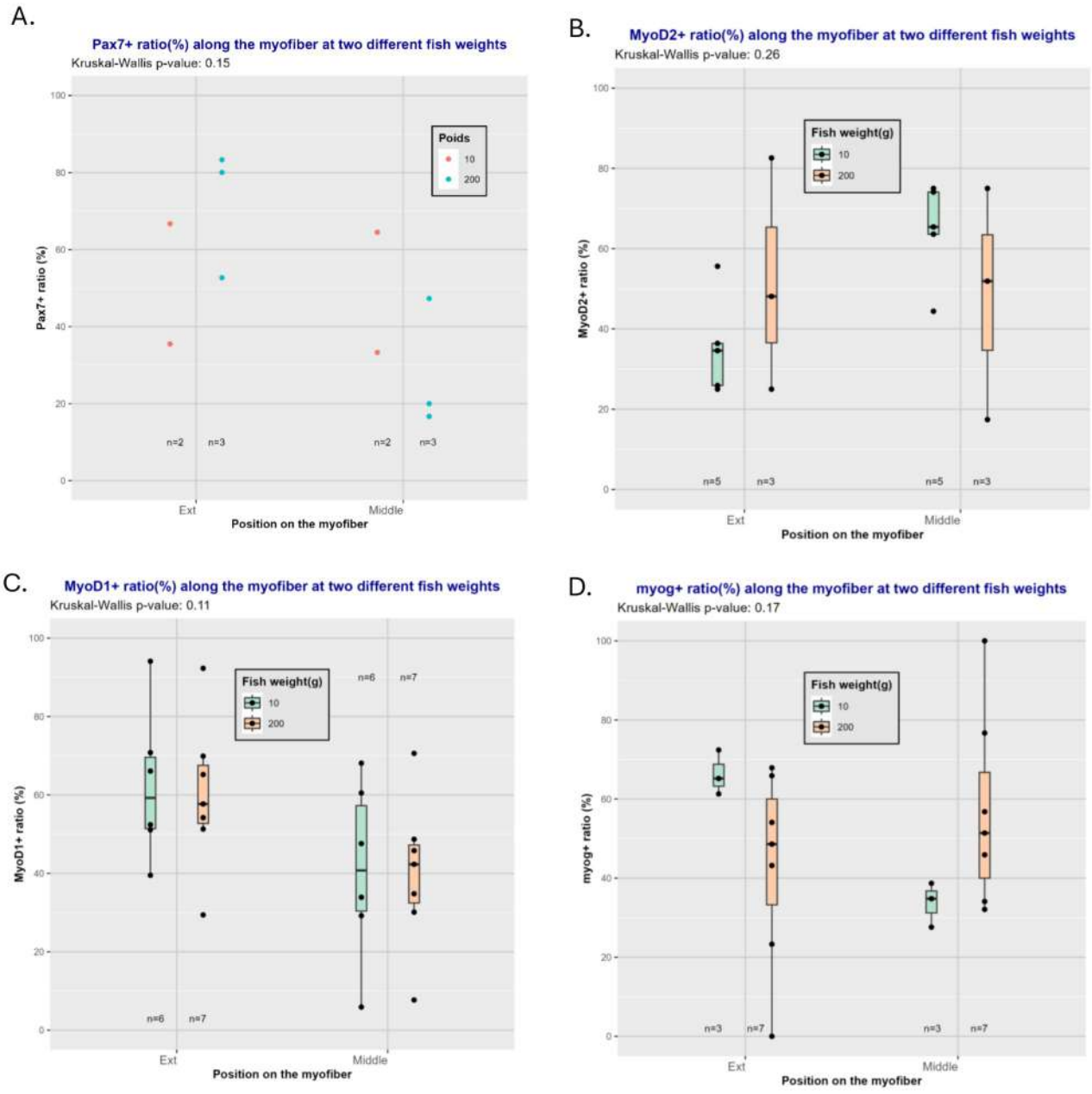

Figure 22 – *<u>Myogenic precursors percentage comparison between fiber's extremities (Ext parameter) and middle of the fibre (Middle parameter) for two fish weight conditions</u>: 10 g and 200 g. A Kruskal-Wallis test was performed for each type of myogenic precursor to make pairwise comparisons between the groups of interest. None of the four non-parametric tests were significative.* ***A.*** *Pax7+ nuclei localization on myofibers (n=5).* ***B.*** *MyoD2+ nuclei localization on myofibers (n=8).* ***C****. MyoD1+ nuclei localization on myofibers (n=13).* ***D****. myog+ nuclei localization on myofibers (n=10).*

4. Discussion

4 .1 A protocol for extraction and isolation of fast-twitched myofibers and 3D-images acquisition has been optimized and validated

To accurately determine the evolution of myonuclear domain and the satellite cell dynamics during the juvenile muscle growth, a protocol to isolate and image whole muscle fiber is a prerequisite.

Muscle fibers have the specificity to be large cells and especially myofibers from trout weighing 600 g or more (diameter>100 µm; length>2 mm). Fiber's transparization was found to be the solution to address the problem of fluorescence signal loss from a certain depth in the z-axis. Given the duration of the acquisitions and the search for a protocol suitable for the larger fibers, only one 3D-image was acquired from 600 g individual as well as from 1000 g individual. These two weight conditions have been removed from analysis to focus only on 10 g and 200 g condition. For a more complete study on myonuclear domain evolution and the satellite cells dynamics and localization during muscular growth, it would be interesting to include heavier fish in the analyses as previous studies revealed a decline in the number of myogenic precursors extracted from muscle of 10 g to 2 kg - trout (Jagot et al., in preparation).
Furthermore, additional work is necessary to increase the number of acquisitions in order to improve statistical power and for allowing more accurate conclusion on a potential effect of trout weight on myogenic precursors' dynamics and MD size evolution.

4.2 Myonuclear domain size is increasing during juvenile muscular growth

We showed that MD size increased significatively between 10 g trout and heavier trout from the 200 g group.
In agreement, total number of nuclei per fiber (from 204 ± 67 to 588 ± 324 *myonuclei* per fiber) and myofiber volume in 10 g and 200 g trout increase. It has already been shown that MD size was not a constant number with a balanced scale between myonuclear accretion and increase of the myofiber volume. In fact, MD size increases during post-natal growth in mice (White et al., 2010).
MD size expansion during juvenile muscular growth would mean myofiber volume expansion is relatively more important than myonuclear accretion. A strong correlation between myofiber diameter and MD size was observed (output of Spearman test gave a p-value of 9.295e-15 and a rho factor of 0.93). This would show the importance of hypertrophy in the balance volume expansion/myonuclear accretion.

Adding other weight conditions (600 g, 1kg, 1.5 kg and 2 kg) to our study would allow us to analyze MD size evolution during adult muscular growth. Indeed, previous work indicate that 2 kg trout muscle contains few satellite cells although fiber hypertrophy takes place suggesting that it may occurs without SC recruitment as previously observed in prepuberal growth in mice (White et al., 2010).

An interesting observation was made while studying the characteristics of the 600 g trout fiber. It showed a low fiber volume (517 x 10^3 μm^3) and low MD size (0.54 x 10^3 μm^3) but a high length (2773 µm) and a high total number of myonuclei (958), positioning this fiber close to the 10 g ones in term of MD. Myofiber length is logically higher than fibers from 10 g group as it is linked to the distance between two myosepta (increasing with individual's size). We can hypothesize that this fiber is a newly formed muscle fiber since post-larval trout growth proceed with both hyperplasia and hypertrophy. Moreover, this small-sized fiber from a heavier trout shows a low MD: hyperplasia process would be linked to strong nuclear accretion.

High standard deviation values of MD size were constated especially in 200 g trout. This could be explained by the mosaic muscular growth that occurs in juvenile trout. Hyperplasia phenomena implies that a large panel of myofibers size can be found, especially for 200 g trout (larger distribution between newly formed myofibers and older ones).
Some of the myofibers from 200 g trout with low diameter were found to have MD values similar to myofiber from 10 g trout (Figure 14). As myofibers from 200 g trout have a higher volume (higher length), this would mean these fibers have a higher number of *myonuclei*. This observation could be explained by the existence of phases of strong nuclear accretion related to the hypertrophic capacity of myofibers.

4.3 No differences were observed in myogenic precursors' percentage during juvenile muscular growth

Regarding results relative to the number of extracted myogenic precursors during juvenile muscular growth (Jagot et al, in preparation), we had supposed that the ratio of myogenic precursors would decrease in myofibers from the 200 g condition, especially for activated satellite cells (SC) or SC in a proliferating stage (Pax7+ and MyoD2+ *myonuclei* analysis). However, no significative differences were found between the two conditions for the four types of myogenic precursors studied (Pax7+, MyoD1+, MyoD2+ and myog+ *myonuclei*). These observations could be explained by the low number of replicates per condition (number of replicates n ranging from two to seven fibers). Moreover, only two weight conditions have been

studied: 10 g and 200 g corresponding to a hyperplasic growth phase. Adding myofibers from older trout in the data set would be necessary.
A surprising result was the relatively high ratio of myogenic precursors per fiber (total mean value being of 15 ± 10 %).
Besides the fact we developed a protocol to detect myogenic probes' positive *myonuclei*, it would be interesting to train a Stardist3D CNN to detect positive nuclei to opal fluorochrome on myofibers' 3D images. This would help to accelerate and improve the reliability of the counting method.

Duplex *in situ* hybridization was validated during the study and all the potential probes' combinations were tested. However, the very low number of observations could not allow us to do statistical analysis of our data. It would be interesting to standardize duplex acquisition to expand the data set size and assign each *myonuclei* to one of the myogenic precursors' clusters revealed by single cell RNAseq analysis (Figure 4). Moreover, the RNAscope Multiplex Fluorescent V2 Assay allows simultaneous visualization up to three different RNA targets per myofiber. An additional probe could be included in the RNAscope protocol to assign even more precisely each myogenic precursor detected to a population.

4.4 Myogenic precursors were evenly distributed on myofibers

We were not able to conclude on a localization pattern of the different myogenic precursors populations studied: no significant differences were found between our two weight conditions. The absence of significative results in our localization analysis could be explained again by our small number of replicates per condition, leading to high standard deviation values and non-normal distribution of our data.
Our initial hypothesis was based on empirical observations under confocal on several fibers showing a higher density of labeled *nuclei* at their ends. We had supposed that a higher proportion of SC would be based on fiber's extremities and at the periphery of fibers under the basal lamina (Fauconneau and Paboeuf, 2001). This could have highlighted potential fusion areas between SC and existing fibers (hypertrophy) or other satellite cells (hyperplasia).
Our second hypothesis was based on a potential myogenic precursors' migration depending on their stage of differentiation. Myocytes would thus be found in a more centered position of myofibers than activated satellite cells.

Moreover, we could refine our regionalization study: fibers were cut in four equal parts in our analysis as an initial approach and for time-saving purposes. A fiber split into ten sections was used in a recent study on myog -/- mutant zebrafish (Ganassi et al., 2020) and could give better

information on SC distribution, especially at fiber's extremities. Changing the number of portions from four to ten could precise our analysis.

Additionally, a follow-up study could focus on localization of SC depending on their fate : it has been shown that two distinct SC populations existed in myofibers depending on whether they were destined to differentiate into muscle cells or to participate in the self-renewal of the SC pool (Collins et al., 2005). Moreover, a more precise analysis could study differential localization within the SC destined to differentiate: a comparison analysis on localization could be made between SC destined to fusion with existing myofibers (hypertrophy) and SC destined to merge with other myogenic precursors (hyperplasia).
This analysis could have an interest to detect SC type and conclude on localization patterns during the different processes of muscular growth at different stages of rainbow trout's life.

4.5 The experimentation and the origin of the fish could have an effect on satellite dynamics

An interesting research perspective would be to study if an intra- or inter-individual effect on satellite dynamics.
Indeed, the tissue sample has always been taken from the same area during tissue dissection that was a two-centimeter white muscle sample above the lateral line (Figure 5). Analyzing myofibers from the ventral part of the white muscle could lead to different conclusions regarding myogenic precursors 'distribution.
Moreover, differences could occur between individuals depending on their genetic origin, sex or position in the tank. A hypothesis could be that fish that stay in the center of the tank do not experience the same current as those on the periphery, leading to different swimming behaviors and potentially different satellite cell dynamics during hypertrophy.
Finally, an effect related to the experimental procedures may exist : there were different batches for each condition as the experiments were repeated over several months.

5. Conclusions and perspectives

This experiment is the first trout's analysis of SC dynamics on fast-twitch extracted and isolated myofibers based on 3D-images acquisition of entire fibers after RNAscope *in situ* hybridization. This protocol was performed and validated in order to detect and count *myonuclei*, especially the ones labeled with opal fluorochrome for myogenic precursors detection at distinct level of differentiations for trout from different weights (that is trout from different ages). Two weight conditions were used for analysis, that is 10g and 200g-weighed trouts, simulating first stages of juvenile muscular growth.
From a methodological point of view, an originality of this work was the fine-tuning training of a convolutional neural network Stardist3D pretrained to detect star-convex shape objects. To our knowledge this CNN was the first trained to detect *myonuclei in 3D.* This experiment proves to be interesting compared to classical methods of stem cells'detection as the use of a neural network ensures additional reliability and a certain speed in the detection of positive nuclei. Moreover, working in 3D allows for the addition of a spatial dimension in this study.

A significative increase of myonuclear domain was observed between myofibers from 10 g condition and 200 g condition ones, refuting the theory of a constant MD size with a balanced trade-off between myofiber volume expansion and nuclear accretion. Thus, it appears that myofiber diameter expansion is the process having the greatest impact on MD size.
Nowadays, we can't conclude on a numeric evolution during juvenile muscular growth of the four types of myogenic precursors studied. Similarly, we cannot conclude on a preferential localization of the different myogenic precursors on myofibers and no migration patterns were seen between our two weight conditions.

The follow-up of this project aims to increase the number of acquisitions and add other weight conditions to the analysis. Other potential effects could be studied as genetic origin of the fish or fiber's diameter for trout from the same age (mosaic muscular growth). Thus, it will be possible to conclude on MD size and SC dynamics at each stage of rainbow trout's juvenile muscular growth under standard breeding conditions, including the potential identification of specificities relative to hyperplasic decline.
Then it will be possible to extrapolate this study by analyzing the impact of breeding conditions on SC dynamics.

References

de Almeida, F.L.A., Pessotti, N.S., Pinhal, D., Padovani, C.R., Leitão, N. de J., Carvalho, R.F., Martins, C., Portella, M.C., Dal Pai-Silva, M., 2010. Quantitative expression of myogenic regulatory factors MyoD and myogenin in pacu (*Piaractus mesopotamicus*) skeletal muscle during growth. Micron 41, 997–1004. https://doi.org/10.1016/j.micron.2010.06.012

Chazaud, B., 2018. Cellules satellites et cellules souches musculaires. Cah. Myol. 11–14. https://doi.org/10.1051/myolog/201817003

Collins, C.A., Olsen, I., Zammit, P.S., Heslop, L., Petrie, A., Partridge, T.A., Morgan, J.E., 2005. Stem Cell Function, Self-Renewal, and Behavioral Heterogeneity of Cells from the Adult Muscle Satellite Cell Niche. Cell 122, 289–301. https://doi.org/10.1016/j.cell.2005.05.010

De Biase, D., Prisco, F., Piegari, G., Ilsami, A., d'Aquino, I., Baldassarre, V., Zito Marino, F., Franco, R., Papparella, S., Paciello, O., 2021. RNAScope in situ Hybridization as a Novel Technique for the Assessment of c-KIT mRNA Expression in Canine Mast Cell Tumor. Front. Vet. Sci. 8. https://doi.org/10.3389/fvets.2021.591961

Fauconneau, B., Paboeuf, G., 2001. 4. Muscle satellite cells in fish. Fish Physiology 18. https://doi.org/10.1016/S1546-5098(01)18005-2

Froehlich, J.M., Galt, N.J., Charging, M.J., Meyer, B.M., Biga, P.R., 2013. In vitro indeterminate teleost myogenesis appears to be dependent on Pax3. In Vitro Cell Dev Biol Anim 49, 371–385. https://doi.org/10.1007/s11626-013-9616-2

Ganassi, M., Badodi, S., Wanders, K., Zammit, P.S., Hughes, S.M., 2020. Myogenin is an essential regulator of adult myofibre growth and muscle stem cell homeostasis. eLife 9, e60445. https://doi.org/10.7554/eLife.60445

Ganassi, M., Zammit, P.S., Hughes, S.M., 2023. Isolation, Culture, and Analysis of Zebrafish Myofibers and Associated Muscle Stem Cells to Explore Adult Skeletal Myogenesis. Methods Mol Biol 2640, 21–43. https://doi.org/10.1007/978-1-0716-3036-5_3

Génevé, L., Bugeon, J., Guyvarc'H, F., Goardon, L., Labbé, L., Gabillard, J.-C., 2022. Croissance du muscle rouge et relation avec la capacité de nage chez la truite arc-en-ciel (Oncorhynchus mykiss). Presented at the 7. Journées de la Recherche Piscicole.

Greek-Walker, M., Pull, G.A., 1975. A survey of red and white muscle in marine fish. Journal of Fish Biology 7, 295–300. https://doi.org/10.1111/j.1095-8649.1975.tb04602.x

Jagot, Sabrina. Caractérisation moléculaire et cellulaire des précurseurs myogéniques du muscle hyperplasique de la truite. Thèse de Biologie Moléculaire et Cellulaire : Université Bretagne Loire.2018.127p.

Jagot, S., Sabin, N., Babarit, C., Bugeon, J., Ralliere, C., Rouger, K., Gabillard, J.-C., 2024. Distinct dynamics of muscle stem cells associated with the hyperplasia decline in trout.

Biology 206, 1337–1351. https://doi.org/10.1242/jeb.00262

Lefèvre, F., Bugeon, J. Déterminisme biologique de la qualité des poissons. 12. Journées Sciences du Muscle et Technologies des Viandes, Oct 2008, Tours, France. ffhal-02752892f

Marras, S., Killen, S.S., Domenici, P., Claireaux, G., McKenzie, D.J., 2013. Relationships among Traits of Aerobic and Anaerobic Swimming Performance in Individual European Sea Bass Dicentrarchus labrax. PLoS One 8, e72815. https://doi.org/10.1371/journal.pone.0072815

Mauro, A., 1961. SATELLITE CELL OF SKELETAL MUSCLE FIBERS. The Journal of Biophysical and Biochemical Cytology 9, 493–495. https://doi.org/10.1083/jcb.9.2.493

McCuller, C., Jessu, R., Callahan, A.L., 2024. Physiology, Skeletal Muscle, in : StatPearls. StatPearls Publishing, Treasure Island (FL).

Mommsen, T., 2001. Paradigm of growth in fish. Comparative biochemistry and physiology. Part B, Biochemistry & molecular biology 129, 207–19. https://doi.org/10.1016/S1096-4959(01)00312-8

Murach, K.A., Fry, C.S., Kirby, T.J., Jackson, J.R., Lee, J.D., White, S.H., Dupont-Versteegden, E.E., McCarthy, J.J., Peterson, C.A., 2018. Starring or Supporting Role? Satellite Cells and Skeletal Muscle Fiber Size Regulation. Physiology (Bethesda) 33, 26–38. https://doi.org/10.1152/physiol.00019.2017

Ralliere, C., 2021. Procédure expérimentale – Hybridation in situ « simple » ou « multiplex » avec la méthode RNAscope : Kit chromogénique et Kit fluorescent (MO-BIO-HIST-018). INRAE, LPGP (document interne).14 p.

Rescan, P.-Y., 2008. New insights into skeletal muscle development and growth in teleost fishes. Journal of Experimental Zoology Part B: Molecular and Developmental Evolution 310B, 541–548. https://doi.org/10.1002/jez.b.21230

Rescan, P.-Y., Rallière, C., Lebret, V., Fretaud, M., 2015. Analysis of muscle fibre input dynamics using a myog:GFP transgenic trout model. Journal of Experimental Biology 218, 1137–1142. https://doi.org/10.1242/jeb.113704

Roman, W., Gomes, E.R., 2018. Nuclear positioning in skeletal muscle. Seminars in Cell & Developmental Biology, SI: Nuclear positioning 82, 51–56. https://doi.org/10.1016/j.semcdb.2017.11.005

Rosser, B., Dean, M., Bandman, E., 2002. Myonuclear domain size varies along the lengths of maturing skeletal muscle fibers. The International journal of developmental biology 46, 747–54.

Schmidt, M., Schüler, S., Hüttner, S., Von Eyss, B., Maltzahn, J., 2019. Adult stem cells at work: regenerating skeletal muscle. Cellular and Molecular Life Sciences 76. https://doi.org/10.1007/s00018-019-03093-6

Schmidt, U., Weigert, M., Broaddus, C., Myers, G., 2018. Cell Detection with Star-Convex Polygons, in: Frangi, A.F., Schnabel, J.A., Davatzikos, C., Alberola-López, C., Fichtinger, G. (Eds.), Medical Image Computing and Computer Assisted Intervention – MICCAI 2018, Lecture Notes in Computer Science. Springer International Publishing, Cham, pp. 265–273. https://doi.org/10.1007/978-3-030-00934-2_30

Steinbacher, P., Haslett, J. r., Obermayer, A., Marschallinger, J., Bauer, H. c., Sänger, A. m., Stoiber, W., 2007. MyoD and Myogenin expression during myogenic phases in brown trout: A precocious onset of mosaic hyperplasia is a prerequisite for fast somatic growth. Developmental Dynamics 236, 1106–1114. https://doi.org/10.1002/dvdy.21103

Stickland, N.C., 1983. Growth and development of muscle fibres in the rainbow trout (Salmo gairdneri). J Anat 137, 323–333.

The state of World fisheries and aquaculture 2024 [WWW Document], n.d. https://doi.org/10.4060/cd0683en

https://doi.org/10.1111/j.1095-8649.2002.tb00898.x

Van der Meer, S.F.T., Jaspers, R.T., Degens, H., 2011. Is the myonuclear domain size fixed? J Musculoskelet Neuronal Interact 11, 286–297.

Weigert, M., Schmidt, U., Haase, R., Sugawara, K., Myers, G., 2020. Star-convex Polyhedra for 3D Object Detection and Segmentation in Microscopy, in: 2020 IEEE Winter Conference on Applications of Computer Vision (WACV). Presented at the 2020 IEEE Winter Conference on Applications of Computer Vision (WACV), IEEE, Snowmass Village, CO, USA, pp. 3655–3662. https://doi.org/10.1109/WACV45572.2020.9093435

White, R.B., Biérinx, A.-S., Gnocchi, V.F., Zammit, P.S., 2010. Dynamics of muscle fibre growth during postnatal mouse development. BMC Dev Biol 10, 21. https://doi.org/10.1186/1471-213X-10-21

Zammit, P.S., Golding, J.P., Nagata, Y., Hudon, V., Partridge, T.A., Beauchamp, J.R., 2004. Muscle satellite cells adopt divergent fates: a mechanism for self-renewal? Journal of Cell Biology 166, 347–357. https://doi.org/10.1083/jcb.200312007

Annex I: Overall protocol for extraction and isolation of entire fast-twitch myofibers and 3D-images acquisition and analysis. The protocol was summarized in six steps, the last one

being 3D-images processing. Step 1 and 2 were adapted from K.Lacquement protocol. Step 4 was adapted from Rallière C. protocol (2021).

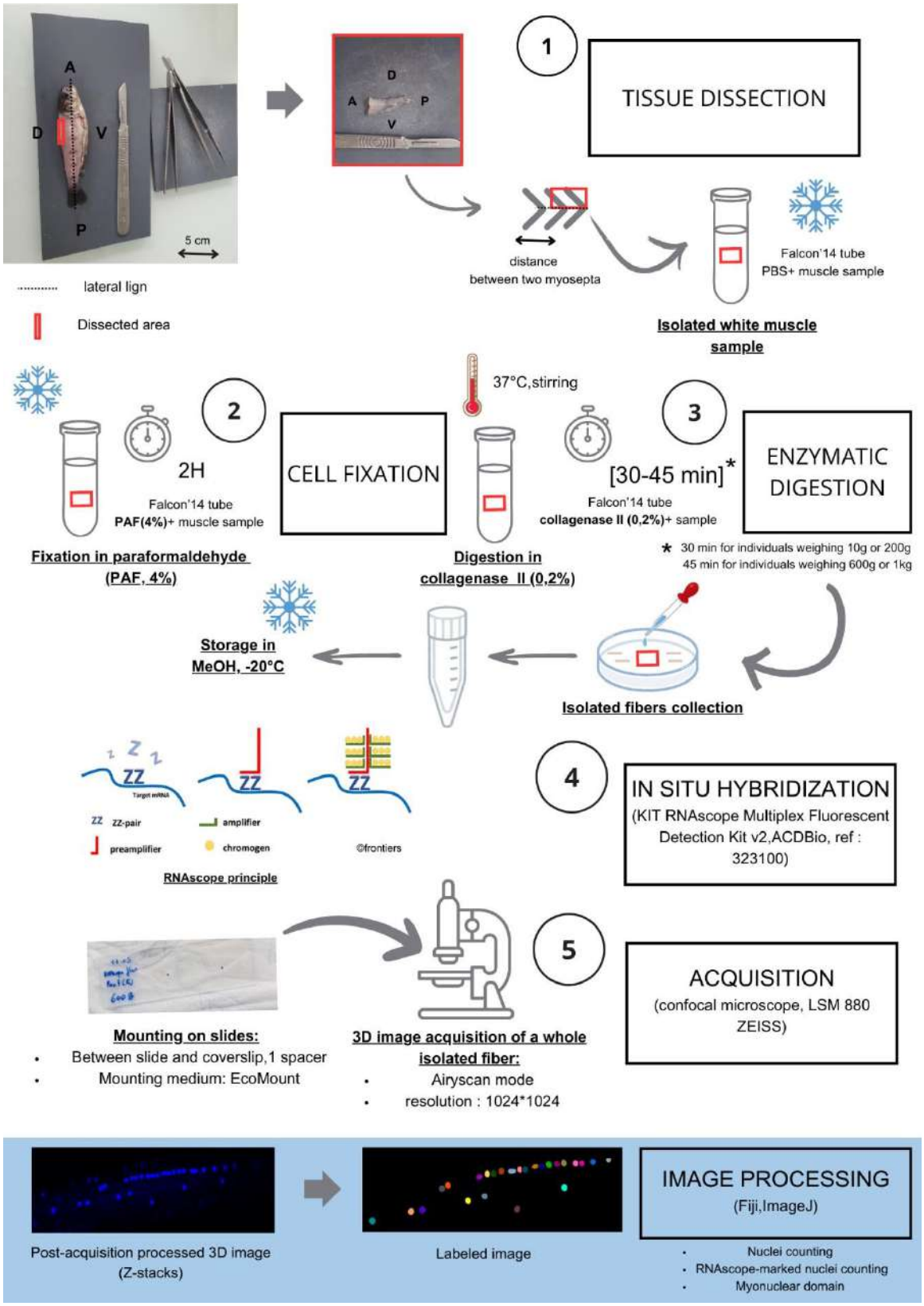

Annex II: Protocol for RNAscope in situ hybridization with Multiplex Fluorescent Reagent V2 Kit (adapted from Rallière C., 2021). The protocol was written in french (intern protocol for the

laboratory). A preliminary step not included in this protocol is fibers'incubation with Protease III (30 min at 40 °C) to maximize tissue permability to probes.

1. Hybridation des sondes RNAscope® et amplification du signal

KIT RNAscope® Multiplex Fluorescent Reagent V2

Equilibrer les réactifs : sortir à TA, les Amp1 à Amp3, blocker, HRP-C1, HRP-C2, HRP-C3 et les Opals.

Rappel des canaux de révélation (C1, C2, C3) des sondes utilisées :

Sonde Pax 7 : C1/C3

Sonde MyoD1 : C2

Sonde MyoD2 : C3

Sonde myog : C3

n.b : l'hybridation duplex MyoD2/myog n'est pas possible.

1) **Préparation des sondes (sous sorbonne) :**

Tenir compte du type de marquage : simple, double ou triple marquage.

Dans le cas d'un double marquage :

Préchauffer les sondes au moins 10 min à 40°C.

Centrifuger brièvement les sondes C2 (ou C3).

Pipetter **1 volume de sonde C2 (ou C3) pour 50 volumes de sonde C1 (1 :50)** dans 1 tube.

Si seules les sondes C2 et C3 sont utilisées, diluer les sondes avec le diluent de sonde (Probe diluent, réf : 300041).

Par exemple : 1µl de sonde C2 (ou C3) pour 50µl de Probe diluent (1 : 50).

Le mélange de sondes peut être conservé à +4°C pendant 6 mois.

2) **Hybridation des sondes RNAscope : hybrider toutes les sondes à multiplexer en même temps.** Bien vérifier que vos sondes aient un canal différent sinon ce n'est pas possible de réaliser un double, triple ou quadruple marquage

-Ajouter 50 µl de mélange de sondes préchauffées (+ ou - selon la taille de la coupe) sur l'échantillon

-Placer les lames dans le four BioBlock.

-Incuber les lames à **40°C pendant 2 H.**

-Lavage dans **1X Wash Buffer** 2 min à RT

-Répéter le lavage dans 1X Wash Buffer 2 min à RT

Remarque : il est possible de faire une pause à cette étape, laisser les lames dans un bain de **SSC5X, O/N à RT**.

Avant de reprendre la manipe, faire **2 lavages 1X Wash Buffer 2 min à RT**

3) **Hybridation Amp1**
-Ajouter 1 goutte d'Amp1 (ou + selon la taille de la coupe) sur l'échantillon
-Placer les lames dans le four HybEZ
-Incuber les lames **30 min à 40°C**
-Lavage dans 1X Wash Buffer 2 min à RT
-Répéter le lavage dans 1X Wash Buffer 2 min à RT

4) **Hybridation Amp2**
-Ajouter 1 goutte d'Amp2 (ou + selon la taille de la coupe) sur l'échantillon
-Placer les lames dans le four HybEZ
-Incuber les lames à **30 min à 40°C**
-Lavage dans 1X Wash Buffer 2 min à RT
-Répéter le lavage dans 1X Wash Buffer 2 min à RT

5) **Hybridation Amp3**
-Ajouter 1 goutte d'Amp3 (ou + selon la taille de la coupe) sur l'échantillon
-Placer les lames dans le four HybEZ
-Incuber les lames à **15 min à 40°C**
-Lavage dans 1X Wash Buffer 2 min à RT
-Répéter le lavage dans 1X Wash Buffer 2 min à RT

6) **Développement du signal HRP-C1 (sondes C1)**
-Ajouter 1 goutte de **HRP-C1** (ou + selon la taille de la coupe) sur l'échantillon
-Placer les lames dans le four HybEZ
-Incuber les lames **15 min à 40°C**
-Lavage dans 1X Wash Buffer 2 min à RT
-Répéter le lavage dans 1X Wash Buffer 2 min à RT
-Eliminer l'excédent de milieu

Préparation des Opals :

-Lors de la première utilisation, les Opals (déshydratées) sont reconstituées avec 75 µl de DMSO puis stockées à +4°C.

-Les Opals sont diluées entre 1 :750 et 1 :3000 dans le tampon TSA fourni avec le kit. La dilution est à ajuster selon l'intensité de fluorescence attendue. Il faut donc tenir compte du taux d'expression du gène.

Commencer avec une dilution moyenne (1 :1500) puis ajuster la dilution pour les manipes suivantes.

-Rajouter **50 µl ou + d'Opal 520 diluée par coupe (ou Opal de son choix).**

Attention : ne pas utiliser le même fluorophore pour plusieurs sondes !

-Incuber **30 min à 40°C.**

-Lavage dans 1X Wash Buffer 2 min à RT

-Répéter le lavage dans 1X Wash Buffer 2 min à RT

-Ajouter 1 goutte de **HRP blocker** (ou + selon la taille de la coupe) sur l'échantillon

-Incuber **15 min à 40°C.**

-Lavage dans 1X Wash Buffer 2 min à RT

-Répéter le lavage dans 1X Wash Buffer 2 min à RT

Remarque : Arrêter à cette étape si vous utilisez juste 1 sonde C1, et procéder au montage des lames

7) Développement du signal HRP-C2 (sondes C2)

-Ajouter 1 goutte de **HRP-C2** (ou + selon la taille de la coupe) sur l'échantillon

-Placer les lames dans le four HybEZ

-Incuber les lames **15 min à 40°C**

-Lavage dans 1X Wash Buffer 2 min à RT

-Répéter le lavage dans 1X Wash Buffer 2 min à RT

-Eliminer l'excédent de milieu

- Rajouter **50µl ou + d'Opal 570 diluée par coupe (ou Opal de son choix).**

Attention : ne pas utiliser le même fluorophore pour plusieurs sondes !

-Incuber **30 min à 40°C.**

-Lavage dans 1X Wash Buffer 2 min à RT

-Répéter le lavage dans 1X Wash Buffer 2 min à RT

-Ajouter 1 goutte de **HRP blocker** (ou + selon la taille de la coupe) sur l'échantillon

-Incuber **15 min à 40°C.**

-Lavage dans 1X Wash Buffer 2 min à RT

-Répéter le lavage dans 1X Wash Buffer 2 min à RT

Remarque : Arrêter à cette étape si vous utilisez juste des sondes C1 et C2, et procéder au montage des lames.

8) Développement du signal HRP-C3 (sondes C3)

-Ajouter 1 goutte de **HRP-C3** (ou + selon la taille de la coupe) sur l'échantillon

-Placer les lames dans le four HybEZ

-Incuber les lames **15 min à 40°C**

-Lavage dans 1X Wash Buffer 2 min à RT

-Répéter le lavage dans 1X Wash Buffer 2 min à RT

-Eliminer l'excédent de milieu

- Rajouter **50µl ou + d'Opal 690 diluée par coupe (ou Opal de son choix).**

Attention : ne pas utiliser le même fluorophore pour plusieurs sondes !

-Incuber **30 min à 40°C.**

-Lavage dans 1X Wash Buffer 2 min à RT

-Répéter le lavage dans 1X Wash Buffer 2 min à RT

-Ajouter 1 goutte de **HRP blocker** (ou + selon la taille de la coupe) sur l'échantillon

-Incuber **15 min à 40°C.**

-Lavage dans 1X Wash Buffer 2 min à RT

-Répéter le lavage dans 1X Wash Buffer 2 min à RT

9) Options avant montage des lames :

***Immunohistochimie (IHC):** une incubation avec un Ac primaire suivie d'une incubation avec un Ac secondaire marqué avec un fluorochrome (Alexa) permet ainsi de visualiser les protéines et les mRNA sur une même coupe.

Les anticorps anti-Myosine MF20, anti-collagen1 ont été testés pour le muscle.

***WGA** : une incubation au WGA marqué par le fluorochrome Alexa 488 permet de visualiser les membranes cellulaires.

10) **Montage des lames :**

-Ajouter 1 goutte de DAPI (contenu dans le kit)

-Incuber 30 sec à TA

-Enlever l'excédent en tapotant la lame sur du papier absorbant

-Ajouter immédiatement 1 ou 2 gouttes de Milieu de montage **Prolong Gold.**

-Placer la lamelle 24 x 50 mm,

-Répéter ces étapes pour chaque lame.

-Laisser polymériser dans une boite noire, 24H à RT et à l'abri de la lumière, lames à plat à l'horizontal.

Stockage des lames à l'abri de la lumière à +4°C.

L'INSTITUT agro Rennes Angers	Diplôme : Ingénieur agronome Spécialité : Sciences halieutiques Spécialisation / option : Aquaculture Enseignant référent : Hervé le Bris

Auteur(s) : DE MONTMORILLON Sophie Date de naissance* : 03/08/2002	Organisme d'accueil : INRAE- Laboratoire de Physiologie et génomique des poissons (LPGP) Adresse : 16A Allée Henri Fabre, 35700 Rennes
Nb pages : 32 Annexe(s) : 2	
Année de soutenance : 2024	Maître de stage : Jean-Charles Gabillard, Jérôme Bugeon

Titre français : Etude de l'évolution du domaine myonucléaire et de la dynamique des cellules satellites au cours de la croissance musculaire de la truite arc-en-ciel.

Titre anglais: Study of the evolution of myonuclear domain and the satellite cell dynamics during the muscle growth of rainbow trout.

Résumé : Comprendre les mécanismes cellulaires à l'œuvre lors de la croissance du muscle blanc de la truite arc-en-ciel est important pour l'optimisation des élevages aquacoles. Nous avons mis au point un protocole d'extraction et d'isolation des myofibres issues de truites de deux poids et âges différents : 10g et 200g. Les myofibres isolées sont marquées par une méthode d'hybridation *in situ* d'ARN par fluorescence afin de localiser les noyaux des cellules satellites, indispensables pour la croissance musculaire. La méthode comprend également l'acquisition d'images 3D de myofibres entières et le décompte des noyaux présents sur les myofibres. Le protocole a été testé et validé pour les deux stades juvéniles étudiés et les cellules satellites ou précurseurs myogéniques ont été étudiés à quatre stades de différentiation. Nous avons mis en évidence une augmentation de la taille du domaine myonucléaire (région transcriptionnelle du cytoplasme) au cours de la croissance musculaire juvénile. Aucune évolution numérique ni localisation préférentielle sur la fibre des quatre stades de précurseurs myogéniques étudiés n'ont été observées. L'augmentation du nombre d'acquisitions d'images 3D de myofibres et l'analyse de la dynamique satellitaire chez des individus ayant des poids plus élevés (truites plus âgées) permettra d'améliorer la représentativité des résultats et de déterminer les caractéristiques cellulaires à l'œuvre lors de la croissance musculaire juvénile de la truite arc-en-ciel.

Abstract: Understanding cellular mechanisms during muscular growth of rainbow trout (white muscle) is fundamental for aquaculture rearing. We have developed a protocol for the extraction and isolation of myofibers from trout of two different weights and ages: 10 g and 200 g. The isolated myofibers are labeled using a fluorescent *in situ* hybridization method to locate the *nuclei* of satellite cells, which are essential for muscle differentiation and growth. The method also includes the acquisition of 3D images of entire myofibers and the counting of *nuclei* located on the myofibers. The protocol was tested and validated for the two juvenile stages studied, and the satellite cells or myogenic precursors were analyzed at four stages of differentiation. We observed an increase in the size of the myonuclear domain (transcriptional cytoplasmic region) of the *myonuclei* during juvenile muscle growth. No numerical changes nor preferential localization on the fiber of the four studied stages of myogenic precursors were observed. Increasing the number of 3D-images acquisitions of myofibers and analyzing satellite dynamics in individuals of a higher weight (older trout) will help improve the relevance of the results and determine the cellular characteristics at work during juvenile muscle growth in rainbow trout.

Mots-clés : Truite arc-en-ciel, croissance, muscle blanc, cellules satellites (CS), précurseurs myogéniques, *myonuclei*

Key Words: Rainbow trout, growth, muscle, satellite cells (SC), myogenic precursors, *myonuclei*